# INFORMATION TO USERS

This manuscript has been reproduced from the microfilm master. UMI films the text directly from the original or copy submitted. Thus, some thesis and dissertation copies are in typewriter face, while others may be from any type of computer printer.

**The quality of this reproduction is dependent upon the quality of the copy submitted.** Broken or indistinct print, colored or poor quality illustrations and photographs, print bleedthrough, substandard margins, and improper alignment can adversely affect reproduction.

In the unlikely event that the author did not send UMI a complete manuscript and there are missing pages, these will be noted. Also, if unauthorized copyright material had to be removed, a note will indicate the deletion.

Oversize materials (e.g., maps, drawings, charts) are reproduced by sectioning the original, beginning at the upper left-hand corner and continuing from left to right in equal sections with small overlaps.

Photographs included in the original manuscript have been reproduced xerographically in this copy. Higher quality 6" x 9" black and white photographic prints are available for any photographs or illustrations appearing in this copy for an additional charge. Contact UMI directly to order.

ProQuest Information and Learning
300 North Zeeb Road, Ann Arbor, MI 48106-1346 USA
800-521-0600

# NOTE TO USERS

**This reproduction is the best copy available.**

UMI®

# Photochemical Hole Burning of Trans-isobacteriochlorin in an n-Octane Matrix

# and

# Resonance Raman Spectroscopy of Mass Selected Metal Clusters in an Argon Matrix

by

**Benjamin L. Davis**

A dissertation submitted to the Graduate Faculty in Chemistry in partial fulfillment of the requirements for the degree of Doctor of Philosophy, The City University of New York

2001

UMI Number: 3008819





Bell & Howell Information and Learning Company
300 North Zeeb Road
P.O. Box 1346
Ann Arbor, MI 48106-1346

This manuscript has been read and accepted for the Graduate Faculty in Chemistry in satisfaction of the dissertation requirement for the degree of Doctor of Philosophy.

4-24-01
Date

Chair of Examining Committee

4-25-01
Date

Executive Officer

Dr. R. Birke

Dr. L. Johnson

Supervisory Committee

The City University of New York

## Abstract

**Photochemical Hole Burning of Trans-isobacteriochlorin in an n-Octane Matrix**

**and**

**Resonance Raman Spectroscopy of Mass Selected Metal Clusters in an Argon Matrix**

by

Benjamin L. Davis

Adviser: Professor John R. Lombardi

The scientific findings that compose this dissertation are divided into two projects. The first deals with the excitation and photochemical hole burning spectroscopy of trans-isobacteriochlorin in an n-octane Shpol'skii matrix at ~ 4.2 K. Principles governing photochemical hole burning spectroscopy will be introduced along with a fully detailed account of the redesigning and computer automation of the experimental apparatus. The excitation and photochemical hole burning spectra

for trans isobacteriochlorin in an n-octane matrix, along with the Stark effect spectra, will be presented and discussed.

The second project presents the resonance Raman spectroscopy of mass selected molybdenum dimer and trimer, aluminum dimer, and chromium timer isolated in argon matrices. For each metal cluster a Resonance Raman spectrum will be presented and discussed. The resonance Raman spectra of these small metal clusters will give insight into the nature of the chemical bonding of the metal molecule under study as well its geometry. A detailed description on the CCNY Metal Clusters Beam will be given in this section. Experimentation in these two distinct fields proved to be a daunting task that produced very interesting results.

*I remember Peewee and Bug's dad, Tyrone.*

**Acknowledgments**

I wish to thank my Lord, Jesus Christ, who died for my sins that I might live eternal, for making me better. Jesus has given me a new life, and I am taking it! All of my past transgressions have been forgiven, and it is his will that shall be done. Through science, we are revealing the secrets of the universe, and I am fortunate to be a part of this. But, love and faith in the Holy Spirit, and not the pursuit of science, have forever altered me.

I am not bitter, angry, nor hate filled at the many people that made this process difficult. I am in this pleasant state because God has filled my life with love. Everyday I feel as if I am dreaming when I see, talk, or remember people that care about Ben: Tyra, Susie, Sipan, Grandma, Peewee, Steve, Kathy, Lombardi, Singh, Peggy, Darrell, Bernard, Jared, J. R., Uncle "T," Uncle Deek, Mrs. Adebowale, Ms. Viv, Ms. Sandra, and my church family at St. John A. M. E. There are too many names and so little time.

To my wife, Tyra, I love who you are and the possibility of who you will become. I look forward to spending the rest of my life with you. My parents, Susie and Sipan, I love you. The Lord blessed me when he gave me you two as parents, and, as I grow

older, friends. Momma, good better best. Never let it rest. Until your good becomes your better, and your better becomes your best. To my dearest heart, Grandma, I remember. *I wish Peewee was here.* Bernard, Jared, and J. R., I miss you. To my mother in law, Peggy, thank you for giving me the most wonderful gift ever, your daughter. To Steve, my mentor, my friend, my brother, I love you. To Singh, strong in mind and in spirit, watching you in the lab was an inspiration, thank you.

Finally, to Dr. John R. Lombardi, where do I begin? Spring 1997, you read my pitiful transcripts and took a gamble. Summer 1997, coffee cup in hand, you introduced yourself to me. "Hi, I'm John Lombardi." From that moment on I traveled the road, and along the way you imparted your experiences about science and life. You never gave up on me. You, my friend, have a kind yet rebellious spirit. It is this that makes you hip and forever young. Thank you, John.

If I have missed anyone, I am sorry, and it is out of my own ignorance. I will end with this: "*As it is written: "For your sake we are killed all day long; We are accounted as sheep for the slaughter." Yet in all these things we are more than conquerors*

*through Him who loved us. For I am persuaded that neither death, nor life, nor angels, nor principalities, nor powers, nor things present, nor things to come, nor height, nor depth, nor any other created things, shall be able to separate us (me) from the love of God which is in Christ Jesus our Lord."* [Rom. 8:36-39].

Peace.

Table of Contents

List of Tables



List of Figures

# Photochemical Hole Burning

## Chapter 1

## 1.1 Introduction

Spectroscopy deals with the concerns of how light changes the natural motions of matter. When light, be it from the sun, a laser, or some sort of lamp, interacts with a molecule, it can be absorbed, scattered, or emitted. When the energy difference between the natural motion (ground state vibration) and a higher energy motion (excited state vibration) is resonant with an incident photon, electrons that are in the ground state will be promoted to the excited state. This action can be measured in the form of an absorption or emission spectrum, which gives the probability of electronic transition between the ground and excited state as a function of the radiant frequency $\nu$. A molecule in the gas phase, experiencing resonant light, will give a spectrum yielding one sharp optical transition, called the purely electronic zero phonon line (PEL) (Fig. 1).[1] As stated above, the frequency of this spectral line represents the energy difference between the ground and excited state divided by Planck's constant:[2]

**Eq. 1.1** $\nu = (E(S_1) - E(S_0))/h$

**Fig. 1.1** Purely electronic zero phonon line of a molecule in gas phase.

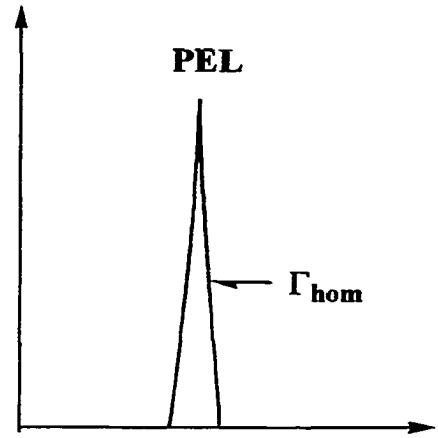


The width of the PEL is called the homogenous line width, $\Gamma_{hom}$, which yields information about the relaxation process of the excited state.[3] The width of this line is determined by optical dephasing interactions that are identical for all molecules under study. When the molecule is in a host matrix, $\Gamma_{hom}$ is defined by the following equation:

$$\textbf{Eq. 1.2}\quad \Gamma_{hom} = (\pi T_2)^{-1} = (2\pi T_1)^{-1} + (\pi T_2^*)^{-1},$$

where $T_1$ is the excited state lifetime and $T_2^*$ is the pure non-radiative relaxation time due to thermally induced fluctuations of the electronic

transition energy.[3] The second term of the equation is a function of lattice vibration scattering and electron and nuclear spin fluctuations.

Guest molecules that are doped into perfect crystal environments, where guest molecules experience identical local environments (Fig. 1.2a), give optical spectra ($\Gamma_{hom}$) that is similar to Fig. 1.1 but is slightly broadened due to guest host interactions (Fig. 1.2b)

**Fig. 1.2** Four guest molecules in a perfect crystal environment experiencing identical local surroundings (a), which gives a ZPL transition (b).

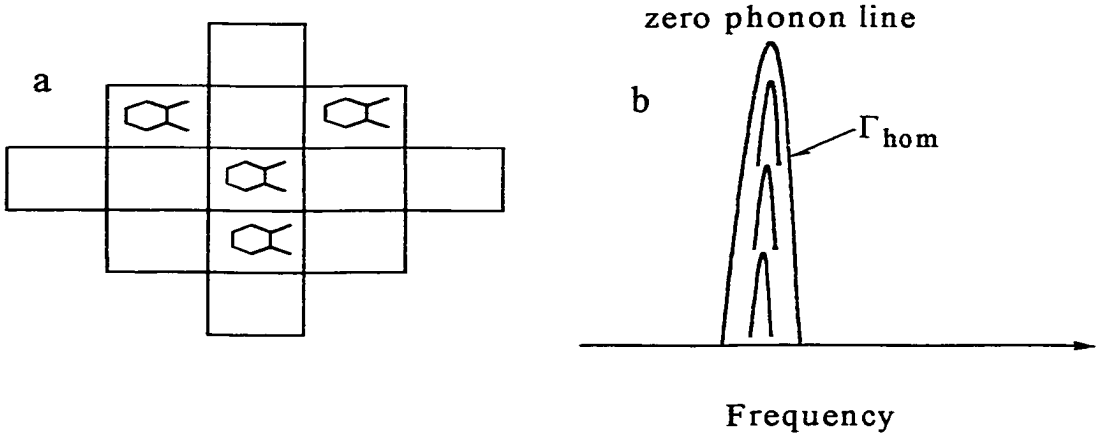


The broadening of $\Gamma_{hom}$ in the perfect crystal matrix is due to vibrational mixing between the guest molecule and the matrix. Vibrations due to the matrix are called phonons. This interaction causes the electronic transition of the guest molecule to be

inhomogeneously broadened ($\Gamma_{inh}$), and gives a spectrum distorting the PEL with a phonon side-band (Fig 1.3). The zero phonon line (ZPL) transition shown in Fig 1.2 is the PEL transition for the four molecules in the matrix with minimal broadening due to phonon interactions. Resolving the ZPL with minor phonon mixing is common for molecules doped in a prefect crystal environment at cryogenic temperatures,[4] but at room temperature ($kT \sim 300$ cm$^{-1}$) there is enough thermal energy to excite phonons of the host matrix.[1,2]

**Fig. 1.3** Depiction of phonon/PEL interaction as a function of temperature. Note that as temperature (T) approaches zero, phonon/PEL interactions decrease and only appear as a slight side band.

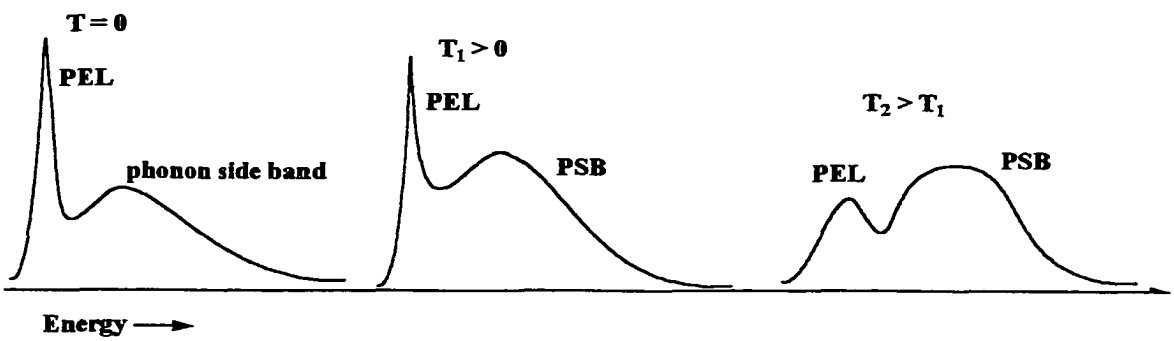


The temperature dependence for guest/phonon mixing is shown in Fig. 1.3. Note that phonon side bands reduce significantly at temperatures below 20 K.

Molecules that are doped into an imperfect crystal will experience slightly different surroundings (Fig. 1.4a). This matrix

effect will cause the ground and excited state energy to vary randomly from molecule to molecule. This random fluctuation also shifts the transition energy of the molecules, giving a distribution of optical transitions for the embedded sample (Fig. 1.4b).

**Fig. 1.4** Guest molecules imbedded in an imperfect crystal. Each experiences a different local environment (a), which results in a distribution of homogeneously broadened transition energies (b).

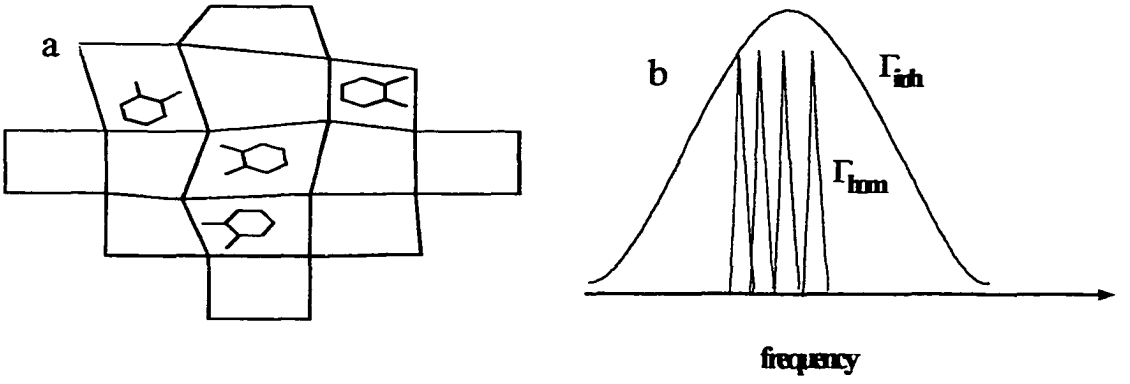


## 1.2 Photochemical Hole Burning

Molecules doped in non-crystalline solids yield a distribution of transitions energies that are typically inhomogeneously broadened. When this occurs, $\Gamma_{hom}$ cannot be readily obtained by normal spectroscopy.[3] One method for probing $\Gamma_{hom}$ in an inhomogeneously broadened spectrum is by saturation spectroscopy. A guest molecule embedded in a host matrix can be probed by radiation of a fixed frequency resonant with the ZPL transition.[5] Radiant saturation of the

system causes resonant molecules to appear as a "hole" or dip in the subsequent absorption or emission spectrum. This saturation method is called photochemical hole burning.

Probing the ZPL by hole burning as a function of different parameters (such as time, temperature, and microenvironments) gives information on the relaxation dynamics of the absorbing molecule as well as guest host interactions. The line width of the burned hole, denoted as $\Gamma_{hole}$, gives insight on the energy of the optically pure transition, and $\Gamma_{hom}$, for the sample molecule. $\Gamma_{hole}$ in the inhomogeneously broadened spectrum can be due to a photochemical process, i.e. phototautomerism in porphryins, where intramolecular chemistry is reversible,[6] or by an irreversible photo-dissociation of the sample molecule.[7] In any event, there is a shift in the natural electronic transition energy transition of the sample molecule (Fig. 1.5). Also note that the photoproduct absorption band is characteristically well separated from the original absorption band. For amorphous hosts, such as glasses, non-photochemical hole burning can occur under the same probing conditions, but the resulting dip in the spectrum is due to a slight structural rearrangement of the local environment of the guest molecule.[3]

**Fig. 1.5** Schematic of PEL transition of gas phase molecule (a) and the shifting of the ZPL transitions after hole burning (b).

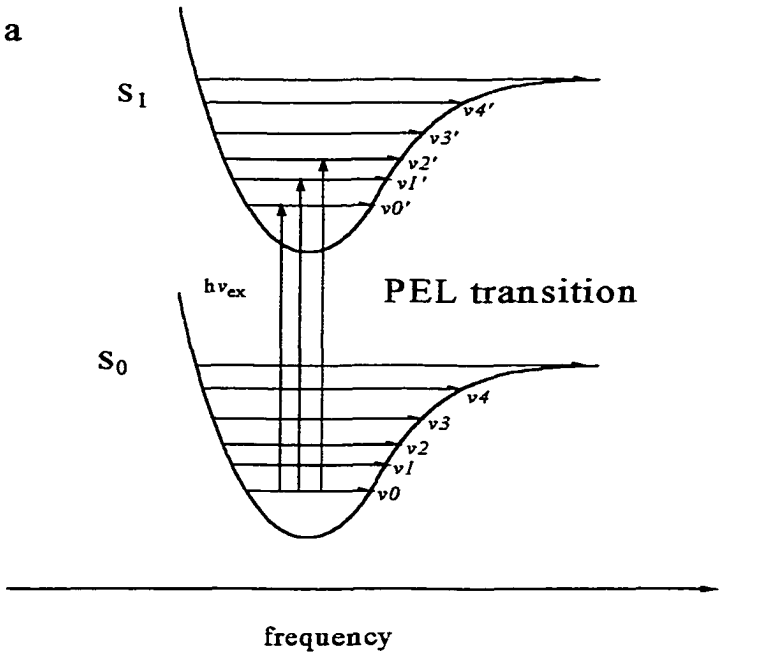


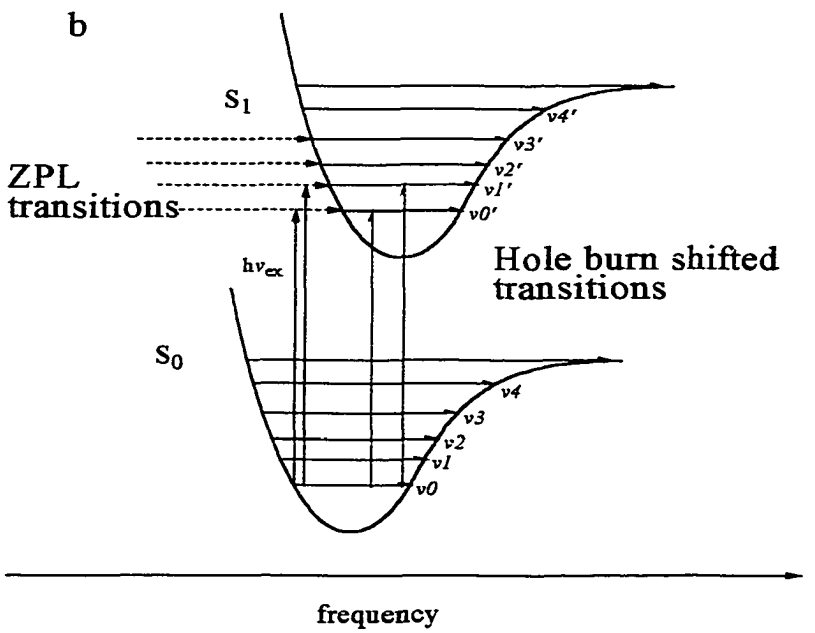

Fig. 1.6 depicts a guest molecule with $\Gamma_{hom}$ doped in a host matrix, thereby causing inhomogeneous broadening of the homogenous line width. Saturating the system with radiation from a narrow lined laser of fixed frequency $\nu_0$ will cause a hole to be burned in the resulting spectrum. The hole in the spectrum (denoted as $\Gamma_{hole}$) is due to photo-degradation or the formation of a photo-derivative of the sample molecule, which absorbs at a different frequency.

The observation of the spectral hole occurs when scanning the burned spectrum with lower intensity laser light in the absorption region of the sample molecule. The width of $\Gamma_{hole}$ will be a function of the width of the exciting laser ($\Gamma_L$). $\Gamma_{hole}$ represents an inverse of $\Gamma_{hom}$ for the guest molecule. To probe an inhomogeneously broadened $\Gamma_{hom}$ via photochemical hole burning, PHB, $\Gamma_L$, the line width of the exciting laser must be less than $\Gamma_{hom}$. At cryogenic temperatures the burned spectral holes are stable, and holes burned and probed at the same temperature gives the relationship of $\Gamma_{hole} = 2\Gamma_{hom}$.[3]

Photochemical hole burning is used in this work to probe $\Gamma_{hom}$ for trans-isobacteriochlorin ($H_2$iBC) in an n-octane matrix. The spectral information obtained gives insight into the lattice orientations for the molecule as it inhabits different sites. Photochemical hole

burning is also used for the application of optical data storage. By doping a polymer or a glass substrate, being divided into pixels or bit spaces, with a photoactive material that undergoes hole burning, a spectral hole can be burned into the substrate.[8] The burned substrate can be used to store bits of information in the form of 1 and 0 or holographic images. A substrate of this sort can be read by more than one color of light due to the varying transition energies of the doped photoactive chromophores, thereby vastly increasing the amount of information that can be stored.

**Fig. 1.6** Spectrum of inhomogeneously broadened $\Gamma_{hom}$ of guest molecule being probed by PHB (a), and the resulting dip in spectrum after saturating $\Gamma_{hom}$ with radiant $\nu_0$.

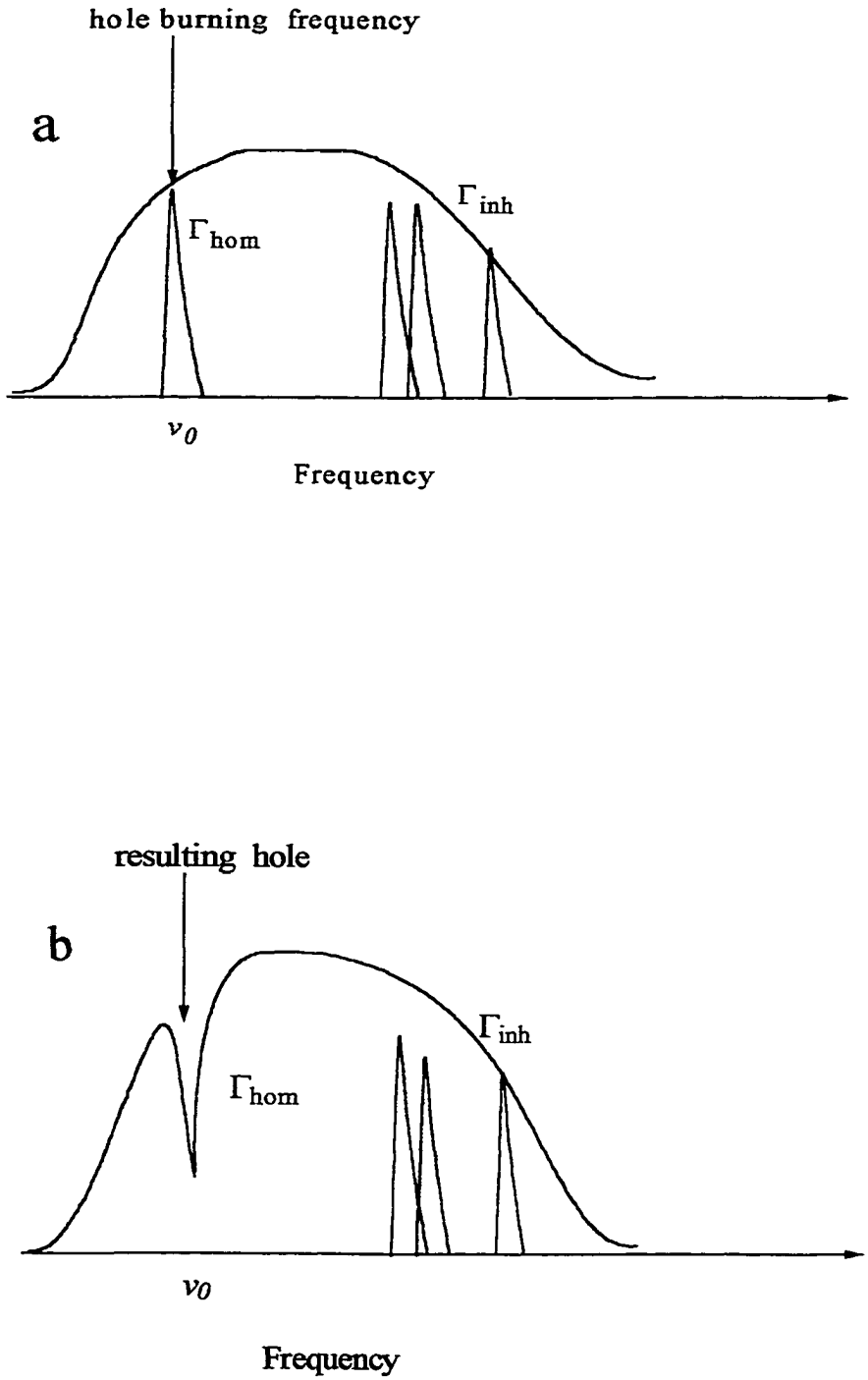

**References- Chapters 1**


1. Huang, W. Y. The total Luminescence Spectrum of Chlorin and Isobacteriochlorin at Low Temperatures. Swiss Federal Institute of Technology: Zürich 1994

2. Rebane, A. "Spectral Hole Burning." www.physics.montana.edu/faculty/rebane October 25, 2000.

3. Völker, S. Annu. Rev. Phys. Chem. 1989, *40*: 499-530

4. Hayes, J. M.; Lyle, P. A.; Small, G. J. J. Phys. Chem. 1994, *98* 7337

5. Ingle, J. D.; Crouch, S. R. Spectrochemical Analysis. Prentice Hall: Saddle River, NJ 1988

6. Völker, S.; Macfarlane, R. M. IBM J. Res. Develop. 1979, *203* 547

7. Devires, H.; Wiersma, D. A. Phys. Rev. Lett. 1976, *36* 91. Devires, H.; Wiersma, D. A. Chem. Phys. Lett. 1977, *51* 565

8. Bains, S. "New glass allows persistent, high-temperature, spectral hole burning." www.spie.org/web/oer/march/mar98/newglass.html. 2000

# Photochemical Hole Burning Apparatus

# &

# Automation of Instrumentation via Data Acquisition

# Hardware and Software Control

## Chapter 2

## 2. 1 Introduction

Initial experimentation concerning hole burning involved the design of an automated spectrophotometer that met the requirement of simultaneously generating and obtaining an excitation spectrum for a molecule in real time under cryogenic conditions. Generation of excitation spectra is done by a series of instrumental components, which include pulsed lasers, fiber optics, focussing lenses, and a photomultiplier tube. As spectral data is generated by these components, the signal is obtained and interpreted via a computer hardware/software (LabView 4.1/NI-DAQ 5.0) interface. The signal acquired by the computer is subsequently plotted in a chart-like program. The computer hardware/software interface is also used to automate specific instrumental components. The following sections of this chapter will detail the instrumentation and computer hardware/software used for garnering hole burning and excitation spectra.

## 2. 2 Experimental Apparatus

Fig. 2.1 is a picture and block diagram of the experimental apparatus. The excitation source consists of a Molectron UV 14

Pulsed Nitrogen Laser, which subsequently pumps a Molectron DL II Series Tuneable Dye Laser. The scanning rate and direction for the diffraction grating housed in the dye laser is controlled by a Molectron DL 245 Scan Grating Control. The average power of the pulsed nitrogen laser is approximately $\geq$ 180 mW. The output from the dye laser is reduced in intensity by $10^{-3}$ by optical density filters, so as not to photo-degrade the sample under study. A single-mode quartz fiber optic, obtained from Newport Inc., carries the dye laser light to the remote sample cell holder.

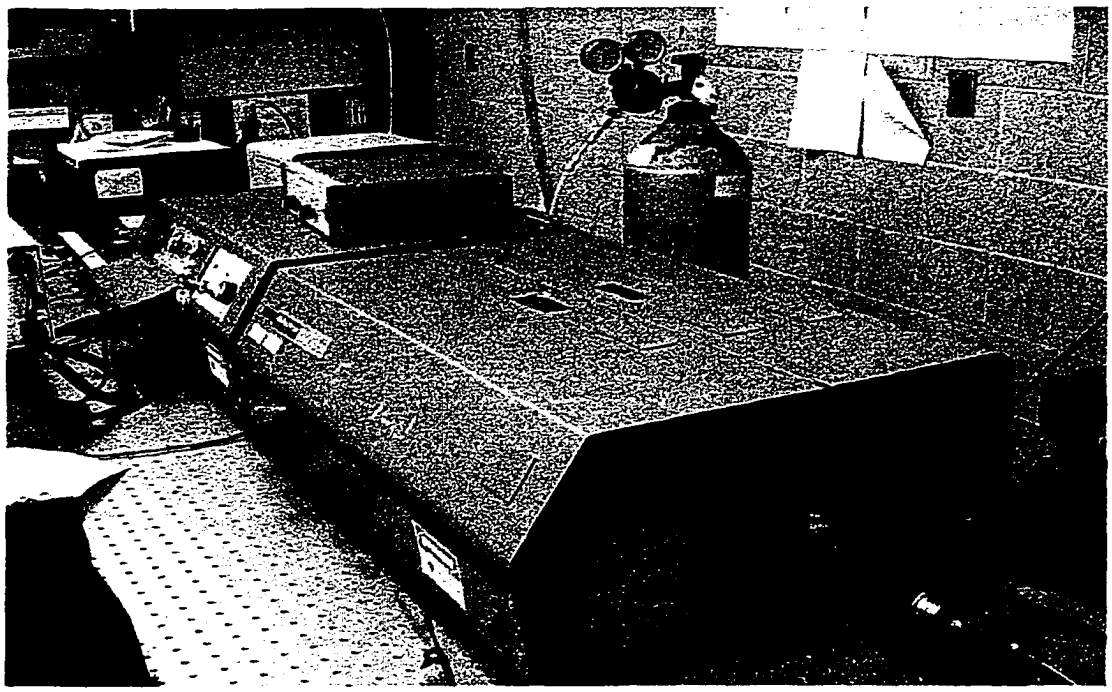

**Fig. 2.1** Picture of hole burning apparatus (above) and an overhead view block diagram of the device (below).

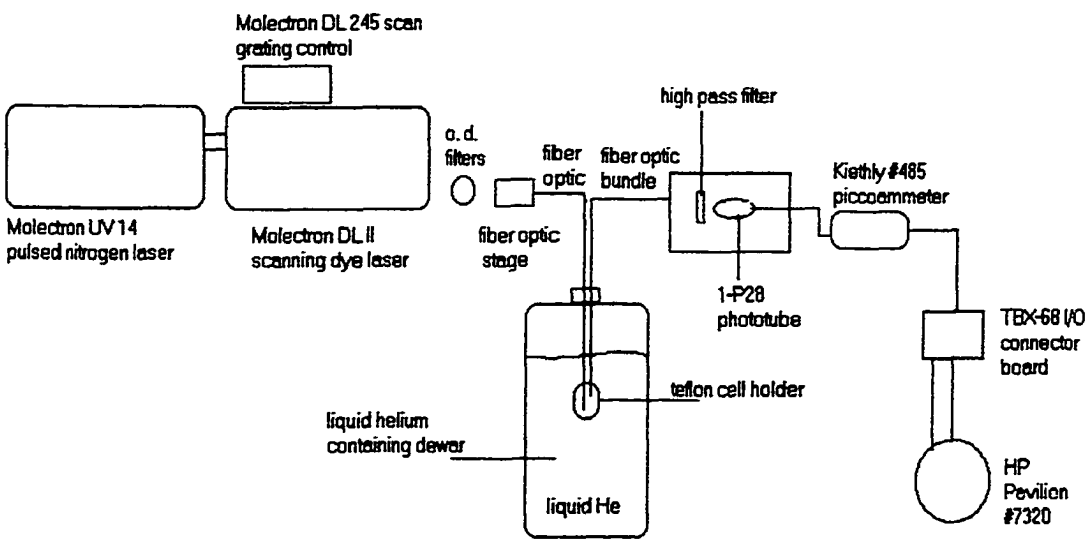

A molecule under study is isolated in a teflon sample cell holder, which is designed to function as a mobile sample compartment (Fig 2.2). The teflon holder contains the output of the quartz fiber optic, focussing and collimating lenses, a high reflectivity mirror, a quartz sample cell, and a fluorescence collimating fiber optic bundle. The cell holder is typically placed in liquid nitrogen or helium dewars, so that remote cryogenic spectroscopy can be performed. The holder focuses the dye laser radiation from the quartz fiber optic with a focussing lens, which has a diameter of 6 mm and an effective focal length of 24 mm, onto a high reflective front silver surfaced mirror, angled at $45^0$ from incident. The exciting light from the high reflective mirror is then directed to the sample quartz cell (with a volume of 1.48 $cm^3$), which is placed at an angle of $90^0$ to the incident laser excitation. The area of the quartz cell that experiences the exciting laser radiation is approximately 6.28 $mm^2$. Sample molecules in resonance with the dye laser radiation in or near the exciting area, will subsequently fluorescence.

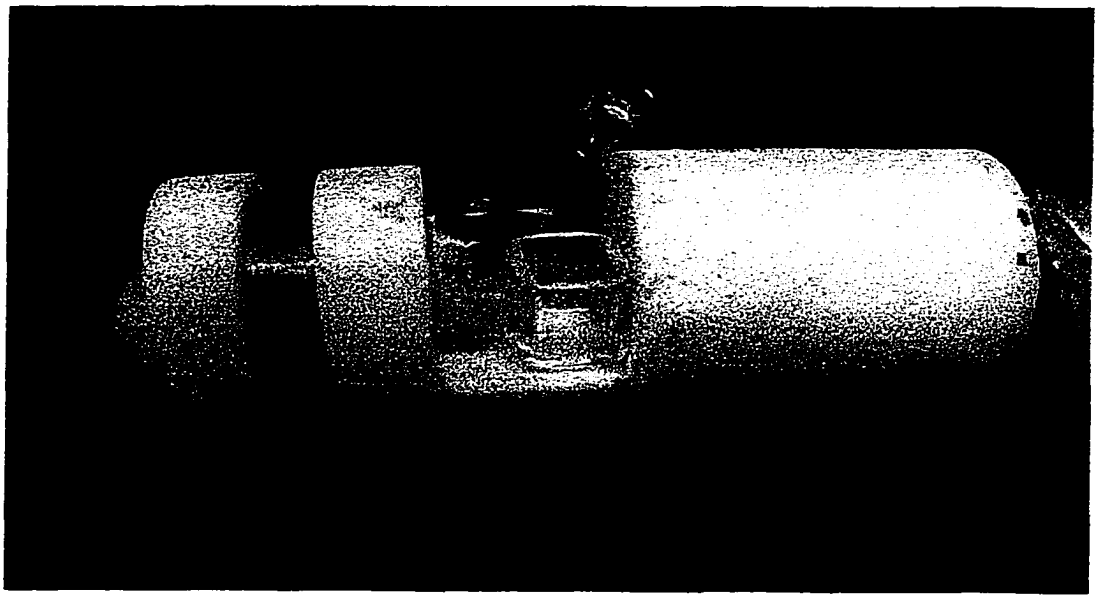

**Fig. 2.2** Picture of the teflon cell holder (above) and overhead view block diagram of the cell (below).

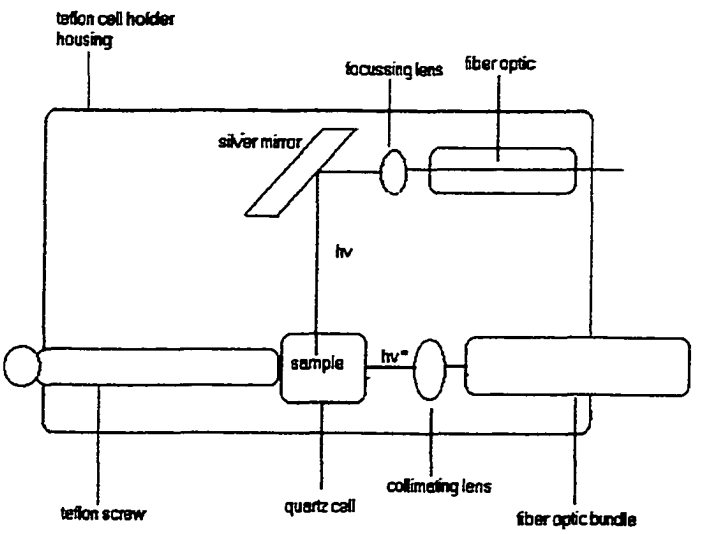

An optical lens with a diameter of 11 mm and an effective focal length of 12 mm collimates the resulting fluorescence. The collimated light is carried to the detection system by a fiber optic bundle. Fluorescence from the fiber optic bundle is passed through an approximately 600 to 615 nm high pass filter. Using the high pass filter ensures the detection system, in the effective filtering region, only detects fluorescence due to excited sample molecules and not from the exciting source laser. The sample fluorescence is detected by a Hamamatsu 1-P28 side on photomultiplier tube (powered at ~ -900 V), which has a working range from 185 to 650 nm (peak $\lambda$ = 340 nm). The detection system, meaning the fiber optic bundle, the high pass filter, and the phototube, are housed in a light-tight metal box. Fluorescence from the sample strikes the phototube, thereby generating a current that is proportional to the detected amount of light. The signal from the phototube, in the form of a negative current, is acquired by an external piccoammeter (Kiethly model #485), where it is converted to a DC voltage. Once this is done, voltages from the piccoammeter are garnered in real time and plotted as a function of the exciting wavelengths, which generates an excitation spectrum.

To apply an external electric filed to a molecule isolated in the quartz cell, a Stark cell can be inserted into the teflon holder. By placing two copper wires into the housing of the teflon holder and connecting the wires to the positive and negative

**Fig. 2.3** Schematic of Stark Cell used to exert an external electric filed across frozen molecules.

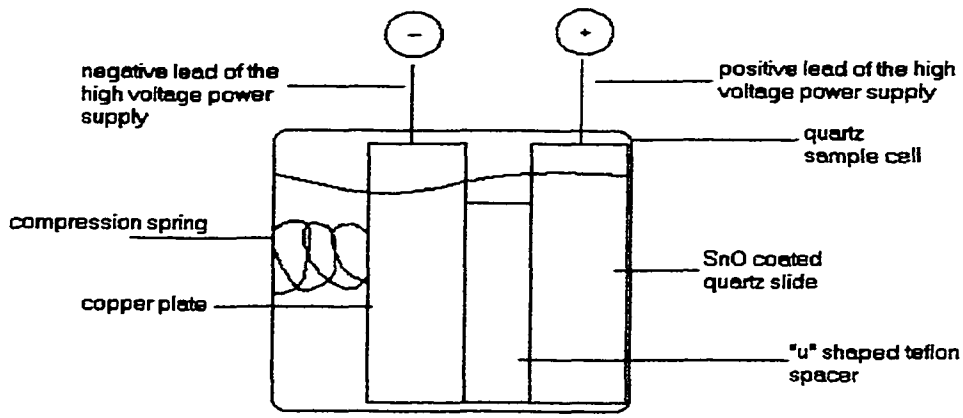


leads of a Glassman 5 kV power supply, and also to electrodes inserted into the quartz sample cell, an external electric filed is generated across the system (Fig 2.3). The positive lead wire is connected to a thin quartz slide, with dimensions 0.88 cm x 1.01 cm and .25 cm thick, coated on one side with tin oxide, with a resistance of $\geq 30\ \Omega$'s (Fig. 3). The negative lead (ground) wire is connected to a copper plate, with dimensions 0.89 cm x 0.89 cm and 0.5 cm thick.

A teflon spacer separates the two electrodes with a thickness of 0.127 cm. The spacer is "u" shaped to allow the exciting light from the dye laser to fully irradiate the area of the sample between the electrodes of the Stark cell. The electrodes separated by the spacer are compressed by a spring. Typical electric field strengths for Stark/hole burning experiments range from 9 to 11.8 $kVcm^{-1}$.

## 2. 3 LabView 4.1/NI-DAQ 5.0 Computer Interface

The hole burning apparatus shown in Figure 2.1 is automated by PC software/hardware control. Parameters from the software/hardware controls the repetition rate of the Molectron UV-14 $N_2$ Laser, the scanning speed and direction of the Molectron DL 245 Scan Grating Control, and acquisition, graphing, and storing of voltages from the Kiethly #485 piccoammeter in spectrum form. The software/hardware systems used to drive these events are LabView 4.1, NI-DAQ 5.0, an AT-MIO-16E-10 interface card, and a TBX-68 I/O connection board. All interfacing components were purchased from National Instruments. The following sections will detail each of the interfacing components and the parameters used to generate and acquire hole burning excitation spectra.

LabView 4.1 is a graphical data acquisition program that has the basic concept of transforming a real instrument into a software based instrument, thereby increasing the versatility of available hardware. The LabView 4.1 is installed on a Hewlett Packard Pavilion 7320 computer with an Intel Pentium processor, using Windows 95 as the operating system. LabView 4.1 allows the user to create front panels that mimic panels of real instruments. A typical LabView 4.1 front panel used in the hole burning experiment is shown in Figure 2.4. This front panel consists of a waveform chart, a boolean stop switch, a file path indicator, and a series of parameters that perform specific tasks during the experiment.

The LabView 4.1 front panel parameters are instructions for an underlying block diagram that executes the desired functions (bottom Figure 2.4). This block diagram is for the front panel of Figure 4. It consists of a series of icons, wires, and virtual instrument programs (VI), which are ready to use programs that can perform a myriad of tasks.

**Fig. 2.4** LabView front panel (above) and corresponding block diagram below)

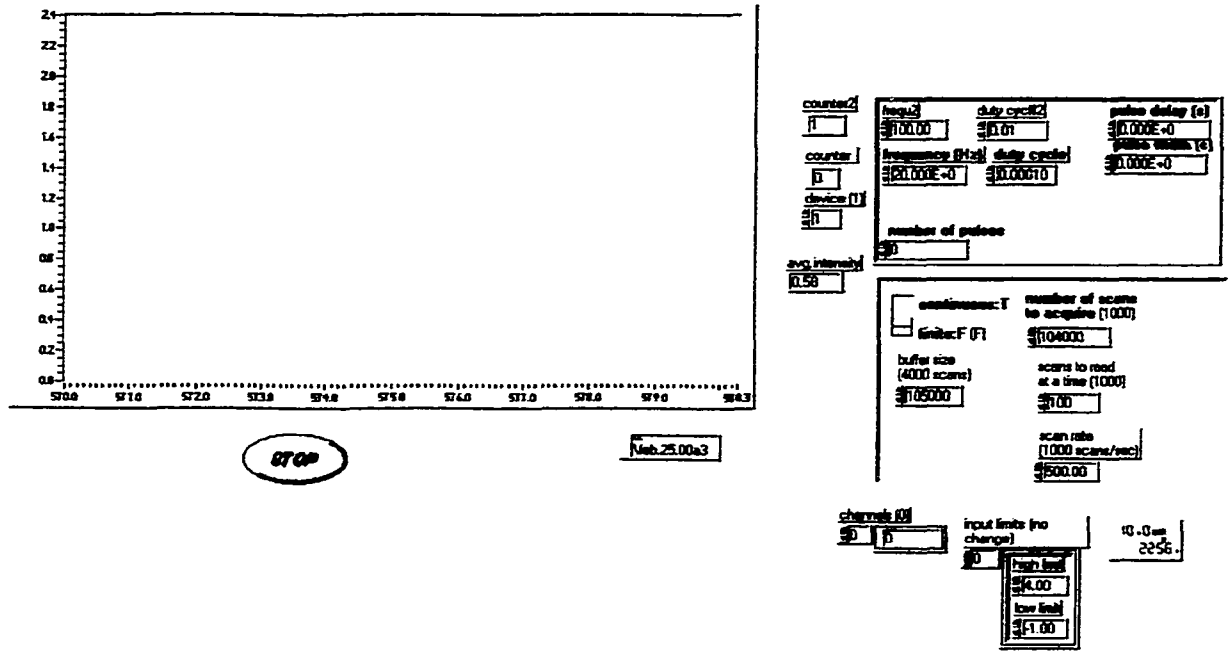


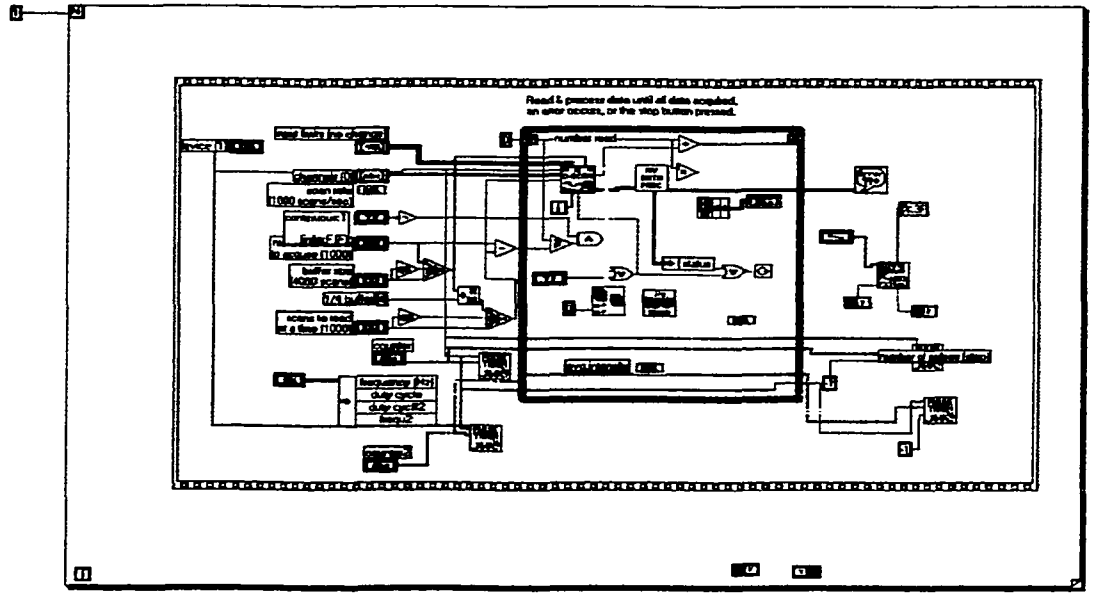

The VIs are located in an expansive DAQ library of LabView 4.1 software. To manipulate the LabView front panel, one only needs a decent working knowledge of the many block diagram icons and the functions of the VIs. The basic task of the block diagram illustrated in Figure 2.4, is to generate two out going square pulses and acquire, and graph, an analog voltage with in a specific time frame. The VIs titled PULSE TRAIN are used to generate the square pulses for this program. The values for the square pulses generated from the PULSE TRAIN VIs are designated on the front panel by frequency and duty cycle parameters. For data acquisition, the VI titled AI C-SCAN is used to acquire a continuous analog voltage. While AI C-SCAN acquires the analog voltage, the program simultaneously shuttles data to an array index where the VI $\mu_x$ MEAN takes the average of the values in the index and then displays the values in graph, "spectrum," form.

An AT-MIO-16E-10 interface board facilitates the ability of LabView 4.1 to generate pulses and receive an analog voltage. This interface board has a 12-bit ADC and DAC with 16 analog inputs, voltage outputs, eight and 32 lines of TTL-compatible digital I/O. The AT-MIO-16E-10 also features two 24-bit counter/timers for

timing I/O. The LabView 4.1 software and the interface board do not communicate directly, but information is passed from LabView to the AT-MIO-16E-10 interface board via the driver software National Instruments Data Acquisition 5.0 (NI-DAQ). The NI-DAQ 5.0 software includes sophisticated techniques for processing data that is stored while new data is acquired.

The outgoing pulses generated by LabView 4.1/AT-MIO-16E-10 interface components, which control the $N_2$ laser, the Scan Grating Control, and the analog signal being acquired from the piccoammeter, are physically passed through a TBX-68 I/O Connector Board. The AT-MIO-16E-10 board connects directly into the SCIX port of the TBX-68 (Fig 2.5). Pin assignments for different functions of the TBX-68 are also shown in Figure 2.5. When the LabView front panel is in run mode, the square pulses generated by the interface board are sent to pins 2 and 40. Connected to these pins are coaxial cables leading to the external outs of the $N_2$ laser and the Grating Scan Control. Connection pin 68 is the designated slot to receive analog voltages from the piccoammeter by a coaxial cable.

**Fig. 2.5** Picture of TBX/68 I-O Connector board (above) and diagram of pin assignments for pins 13-47 (below).

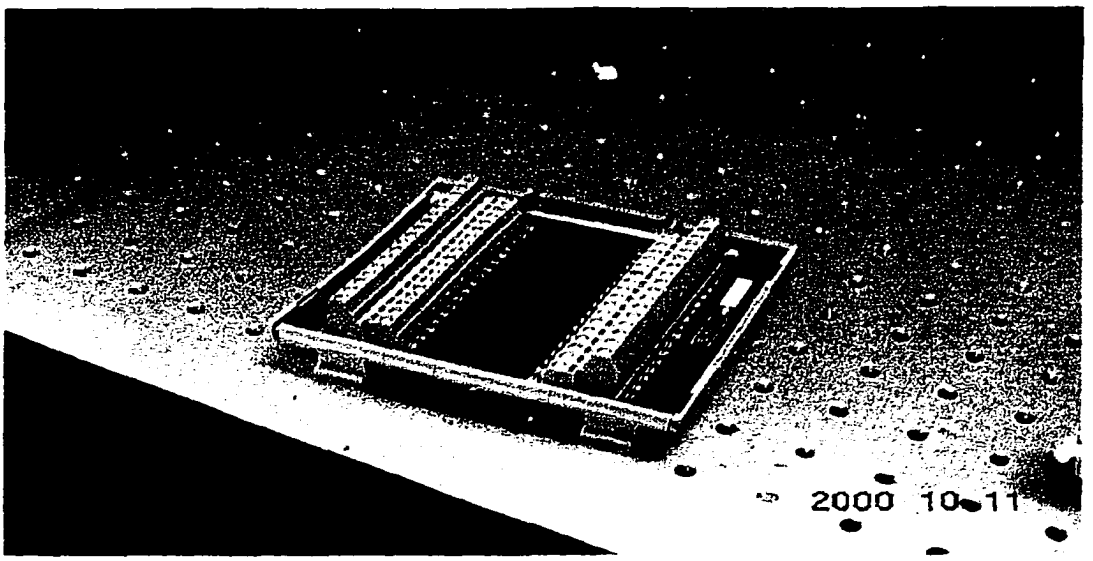


| | | | |
|---|---|---|---|
| ACH8 | 34 | 68 | ACH0 |
| ACH1 | 33 | 67 | AIGND |
| AIGND | 32 | 66 | ACH9 |
| ACH10 | 31 | 65 | ACH2 |
| ACH3 | 30 | 64 | AIGND |
| AIGND | 29 | 63 | ACH11 |
| ACH4 | 28 | 62 | AISENSE |
| AIGND | 27 | 61 | ACH12 |
| ACH13 | 26 | 60 | ACH5 |
| ACH6 | 25 | 59 | AIGND |
| AIGND | 24 | 58 | ACH14 |
| ACH15 | 23 | 57 | ACH7 |
| DAC0OUT[1] | 22 | 56 | AIGND |
| DAC1OUT[1] | 21 | 55 | AOGND |
| EXTREF[2] | 20 | 54 | AOGND |
| DIO4 | 19 | 53 | DGND |
| DGND | 18 | 52 | DIO0 |
| DIO1 | 17 | 51 | DIO5 |
| DIO6 | 16 | 50 | DGND |
| DGND | 15 | 49 | DIO2 |
| +5V | 14 | 48 | DIO7 |
| DGND | 13 | 47 | DIO3 |

The normal experimental parameters employed to externally trigger the $N_2$ pulse laser at 20 pulse/sec are a 20 Hz frequency with a duty cycle value of 0.001. The frequency and duty cycle parameters of the front panel shapes out going square pulses, TTL pulses ranging from 0 to ± 5 V which controlling the repetition rate of the $N_2$ laser and the rate at which the dye laser is scanned, by specifying ratios between the pulse phase and the delay phase of the square pulse. Parameters for externally controlling the Molectron DL 245 Scan Grating control scans the grating of the dye laser at a rate of ~ 0.826 $cm^{-1}$/sec. The waveform chart acquisition parameters control the rate and quantity of the data acquired. A separate LabView 4.1 program determines the direction of scanning by sending an analog ± 5 V signal to the up/down input of the Molectron DL 245 Scan Grating control. The signal limits parameter controls the upper and lower limits of the voltages that are acquired from the piccoammeter. The device parameter gives the address (port) of the AT-MIO-16E-10 interface board in the HP Pavilion 7320. Counter 1 and counter 2 are designators for the interface card and the I/O connection board for the outgoing square pulses.

# Excitation, Hole-Burning, and Stark Spectroscopy of Free Base Isobacteriochlorin in an n-Octane Matrix at Liquid Helium Temperatures

## Chapter 3

## 3.1 Introduction

Free base isobacteriochlorin ($H_2$iBC) is an isomeric form of bacteriochlorin. In the latter molecule, two pyrrole rings with reduced exterior double bonds are opposite each other, but $H_2$iBC consists of two pyrrole rings with reduced double bonds that are adjacent to one another. At room and cryogenic temperatures, $H_2$iBC exists in two stable tautomeric forms, cis and trans (Fig. 3.1).[1]

**Fig. 3.1** Trans-isobacteriochlorin. Note that the inner protons can inhabit two positions.

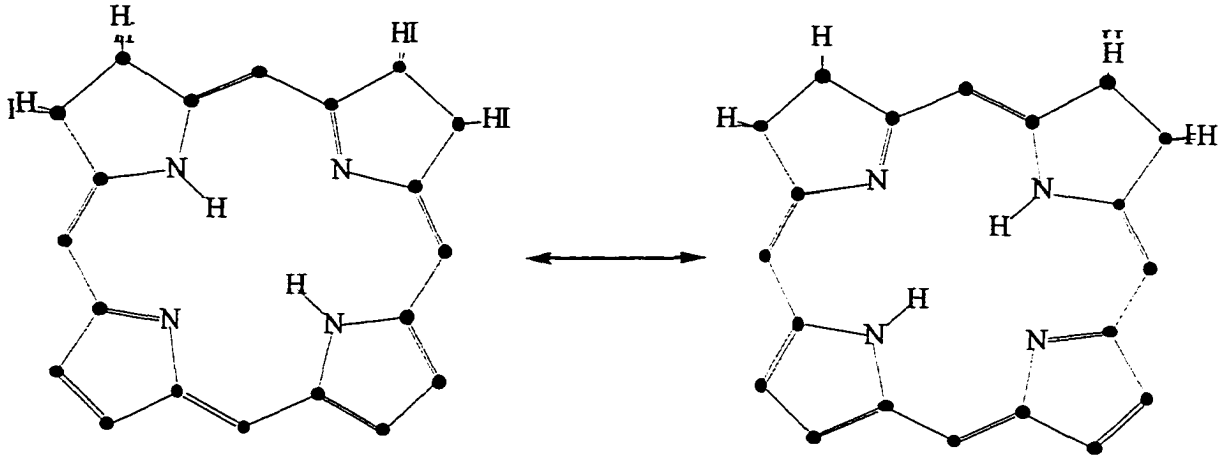

The trans form of $H_2$iBC readily undergoes photochemical hole burning by a $90^0$ rotation of the inner protons of the molecule.[2] When a dilute solution of $H_2$iBC in n-octane is slowly grown into a single crystal, the excitation spectrum of the system displays several peaks belonging to a single site (A).[2] When $H_2$iBC is rapidly cooled in an n-

octane Shpol'skii matrix, as with our experiment, the subsequent excitation spectrum yields a different group of lines assigned to a second type of site (B). A and B sites for $H_2$iBC in the n-octane Shpol'skii matrix appear in the 0-0 optical transition region for this molecule (580 nm region).[1]

The observation of both types of sites in our excitation spectrum for $H_2$iBC in a n-octane Shpol'skii matrix is in keeping with experimental results obtained by S. Voelker et al.[3,4,5] and G. Jansen et al.[6] Their experiments documented that porphyrin type molecules can inhabit two sites when rapidly cooled in certain n-paraffins. Note that, Jansen et al.[6] observed a photophysical change of site B in the fluorescence spectrum of palladium porphin in a heptane single crystal. During the course of their experiment, they observed the gradual formation of new spectral lines associated with site B, which they denote as site B′. It was unknown to them at the time whether or not these lines were formed by a thermally activated process, or whether they were created due to the absorption of light.

In this work, we examine changes in the excitation spectrum of $H_2$iBC in an n-octane Shpol'skii matrix by way of photochemical hole burning and the Stark effect. In our excitation spectrum, each site (A

and B) consists of four intense spectral lines. The hole burning spectra for $H_2$iBC gives evidence that site A in the n-octane single crystal[2] is identical to site A in the n-octane Shpol'skii matrix. For $H_2$iBC in the n-octane single crystal only site A persists. It is only upon rapid cooling of the $H_2$iBC/n-octane matrix that site B forms.

Lines representing site B in the Shpol'skii system are also examined by photochemical hole burning. When specific peaks of site B are illuminated with strong laser radiation, four new lines form in the subsequent excitation spectrum. Upon burning the initial excitation lines of site B and forming the four new lines, we further observe that burning in spectral lines of site B increases the intensities of certain spectral lines attributed to site A. The $H_2$iBC Shpol'skii system is also subjected to an external electric field while scanning the excitation source. From the Stark effect we observe minimal broadening for spectral lines in site A, but site B exhibits a lowering of intensities of the four new lines. We examine the implications of photochemical hole burning and Stark spectra of sites A and B for the orientations of $H_2$iBC in the n-octane matrix.

### 3.2 Experimental

Free base isobacteriochlorin ($H_2$iBC) was synthesized using the methods of Egorova et al.[7] A dilute solution (~$10^{-6}$ M) of $H_2$iBC in n-octane is rapidly cooled in a liquid nitrogen bath, while contained in a square quartz cell, and quickly transferred into a tank of liquid helium. The excitation spectrum of trans-$H_2$iBC is garnered using a Molectron DL II tunable dye laser (with a bandwidth 0.30 $cm^{-1}$ and an average laser power of ≤ 180 mW), which is pumped by a Molectron UV 14 nitrogen laser. The dye laser emission is focused onto a quartz fiber optic strand obtained from Newport Inc., which transports the excitation radiant to the sample. During scanning, the laser emission from the Molectron DL II dye laser is reduced by ~ $10^{-3}$ of the full laser power via optical density filters, to prevent the photo bleaching of the trans-isobacteriochlorin sample. For photochemical hole burning, the optical density filters are removed for 60 to 120 seconds while the dye laser is fixed at the maximum of the spectral line of interest. The irradiated sample area is ~ 6.38 $mm^2$.

Fluorescence from the excited trans-$H_2$iBC is collimated by a quartz lens and focused onto a fiber optic bundle. The $H_2$iBC

fluorescence is the passed through an ~ 600 nm high pass filter, which is detected by a Hamamatsu 1P28 side-on photomultiplier tube. After which, the data is collected in real time by LabView 4.1 software.

A Stark cell is constructed for application of an external electric field to the system. The Stark cell consists of a thin quartz slide, ~ 0.25 cm thick, coated on one side with tin oxide, which is optically transparent for collection of fluorescence. The effective area of irradiation in the Stark cell is ~ 5.25 $mm^2$. The electric field is generated by a Glassman high voltage power supply, where the maximum voltage output is 5 kV.

### 3.3 Results

The excitation spectrum of trans-$H_2$iBC in an n-octane Shpol'skii matrix at 4.2 K is shown in Fig. 3.2. The excitation spectrum displays two sets of spectral peaks labeled site A and B. Both sites are examined by photochemical hole burning to obtain a better understanding of how the guest $H_2$iBC molecules orient in the host n-octane Shpol'skii matrix.

**Fig. 3.2** Excitation spectrum of trans-$H_2$iBC in an n-octane matrix before (a) and after (b) burning line b2.

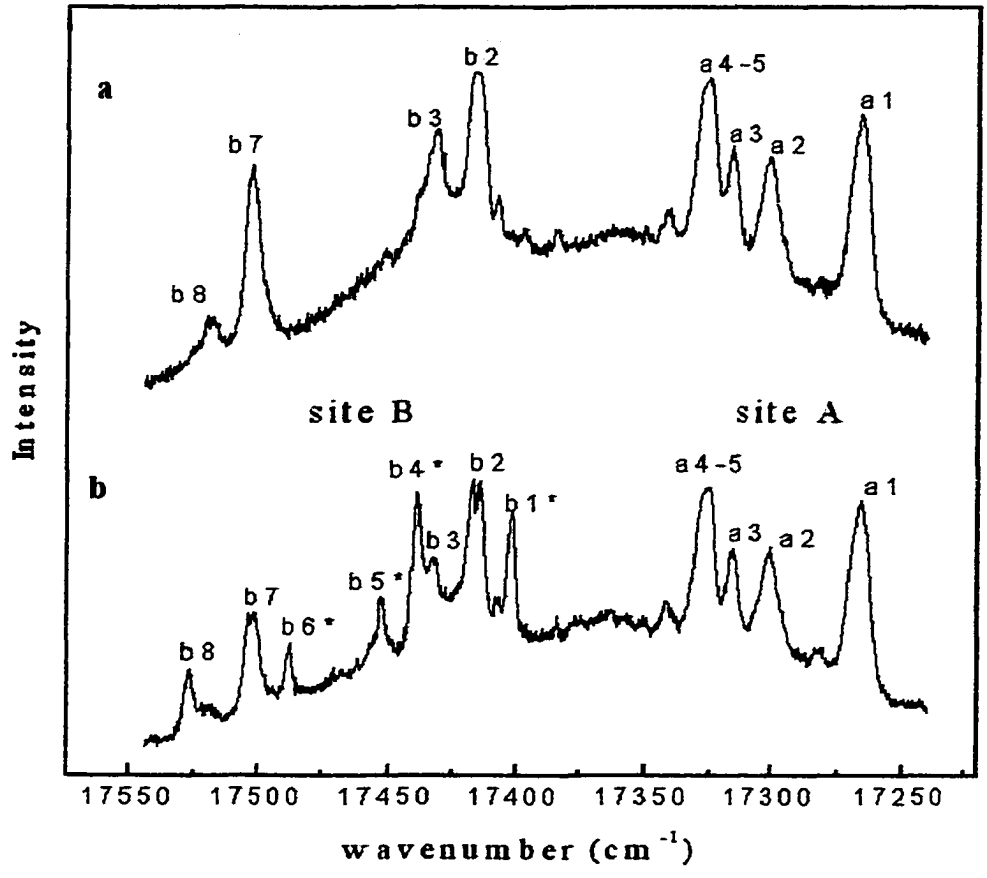


The excitation spectrum of site A displays four intense spectral peaks in the spectral range of ~ 17,300 $cm^{-1}$ to 17,200 $cm^{-1}$ (Figure 3.2a). In the direction of increasing wavenumbers, these four peaks are labeled a1, a2, a3, and a4-5. The maxima of these peaks are given in Table 3.1.

**Table 3.1.** Spectral peak positions of site A

| Spectral Peaks | Frequency ($cm^{-1}$) |
|---|---|
| a1 | 17,224 |
| a2 | 17,259 |
| a3 | 17,275 |
| a4-5 | 17,284 |

From the frequencies at which the four spectral peaks reside in our excitation spectrum, it is assumed that these peaks are analogous to the five spectral peaks acquired by Johnson et al. for trans-$H_2$iBC in the single crystal form of n-octane.[2] The only discrepancy is that the fourth and fifth peaks of the previous work were partially resolved. These lines in our excitation spectrum are, most likely, unresolved due to an increase in inhomogenous broadening brought on by greater guest host interactions in the Shpol'skii lattice.

Upon illuminating spectral peak a1, spectral peak a4-5 increases in intensity and vice versa. Molecules that are in resonance with the hole burning frequency appear in the subsequent excitation spectrum as a dip in the a1 spectral line. The hole in spectral line a1 is roughly the same as the bandwidth of the dye laser, ~ 0.3 $cm^{-1}$, which is possible since the width of spectral peak a1 is ~ 7.3 $cm^{-1}$.

The hole created in spectral line a1 is "filled in" when the burning procedure is performed at the peak of the a4-5 spectral line. This reversible relationship is also exhibited between spectral lines a4-5 and a3. The spectral lines of site B are unaffected when probing site A by photochemical hole burning. Due to the coincidence of the spectral positions and separation distance of the photochemically paired lines and the hole burning patterns exhibited for site A, we believe that our site A of $H_2$iBC in the n-octane Shpol'skii matrix is identical to that of site A in the n-octane single crystal acquired by Johnson et al.[2]

Because the environment of the molecules in site A is symmetric, Johnson et al.[2] argued that there would be distinct spectral lines for the two trans tautomers. They also reasoned that the photochemically paired lines were due to specific molecular orientations of $H_2$iBC in the crystal lattice. Spectral peak a2 does not show any visible effects from the photochemical hole burning process. The inability to burn spectral peak a2 was also observed by Johnson et al. for this molecule in the single crystal.[2] They raised the possibility that spectral peak a2 displays no hole burning features due to the coincidence of several spectral lines caused by a totally symmetric

environment experienced by the guest molecule in the host lattice.[2] Because of the previous hole burning results of site A for $H_2$iBC in the single crystal, our experimentation will focus on $H_2$iBC molecules in site B and their unique relationship to $H_2$iBC molecules in site A.

Site B of the excitation spectrum of trans-$H_2$iBC initially displays four spectral peaks, which do not appear in the single crystal spectrum. In the direction of increasing wavenumbers the spectral lines are designated b2, b3, b7, and b8, in the spectral range of ~ 17,475 $cm^{-1}$ to 17,330 $cm^{-1}$ (Figure 3.2a). The wavenumbers at which these peaks appear are given in Table 3.2.

**Table 3.2.** Spectral positions of site B. b* lines appear after burning unstarred lines.

| Spectral lines | Frequency ($cm^{-1}$) |
|---|---|
| b1* | 17,360 |
| b2 | 17,374 |
| b3 | 17,390 |
| b4* | 17,397 |
| b5* | 17,411 |
| b6* | 17,445 |
| b7 | 17,460 |
| b8 | 17,485 |

The spectral lines of site B are probed via photochemical hole burning in an identical manner to the hole burning process used to probe site A. Fixing the dye laser emission at ~ 17,374 $cm^{-1}$, peak b2, and exposing the sample to the full laser power for sixty seconds, yields an excitation spectrum that contains four new lines (Figure 3.2b). Burning any of the spectral lines of site B forms the new spectral lines, but they display greater intensity when formed by burning at line b2. In the direction of increasing wavenumbers the four new spectral lines are designated b1*, b4*, b5*, and b6*. Note that, spectral line b8 appears weakly in the initial excitation spectrum but increases upon the formation of the b* spectral lines, which causes this line to shift in spectral position.

The formation of the b* lines for $H_2$iBC in an n-octane Shpol'skii matrix is a similar phenomenon detected by Jansen et al.[6] While studying the Zeeman shifts of excited palladium porphin in a heptane single crystal, they initially detected two sites in their single crystal system, site A and B. During the course of their experimentation, they observed the gradual formation of new spectral peaks associated with site B. They assigned the new lines as belonging to a different site, B′, that is coplanar to site B, and the

formation of the lines is due to an in plane rotation of over $20^0$ of the trapped molecule. It was unknown to them at the time whether or not these new line were formed via a thermally activated process, or were created by the absorption of light.[6]

Photochemical hole burning experiments on the newly formed lines of site B display photochemical relationships that seem, on first inspection, chaotic. Burning at the maximum of any unstarred spectral line, meaning line b2, b3, b7, or b8, readily forms the four new lines of site B. Forming the new lines burning line b2, we observe a spectral hole in line b2 as well as an overall decrease in intensity of all unstarred lines in site B. This phenomenon was also observed for the new lines of site B as well. By this we mean burning any starred spectral line in site B will decrease the intensity of all starred lines but will increase the intensity of all unstarred lines in site B.

Once all starred lines are formed by hole burning, certain spectral lines of site B could photochemically interconvert with spectral lines of site A. This is shown in Figures 3.3 (a) and (b). In Figure 3(a), spectral lines a1, a3 and b8 are photochemically burned.

**Fig 3.3** Resulting excitation spectrum after burning spectral peaks a1, a3, and b8 (a) and after burning peak b1*

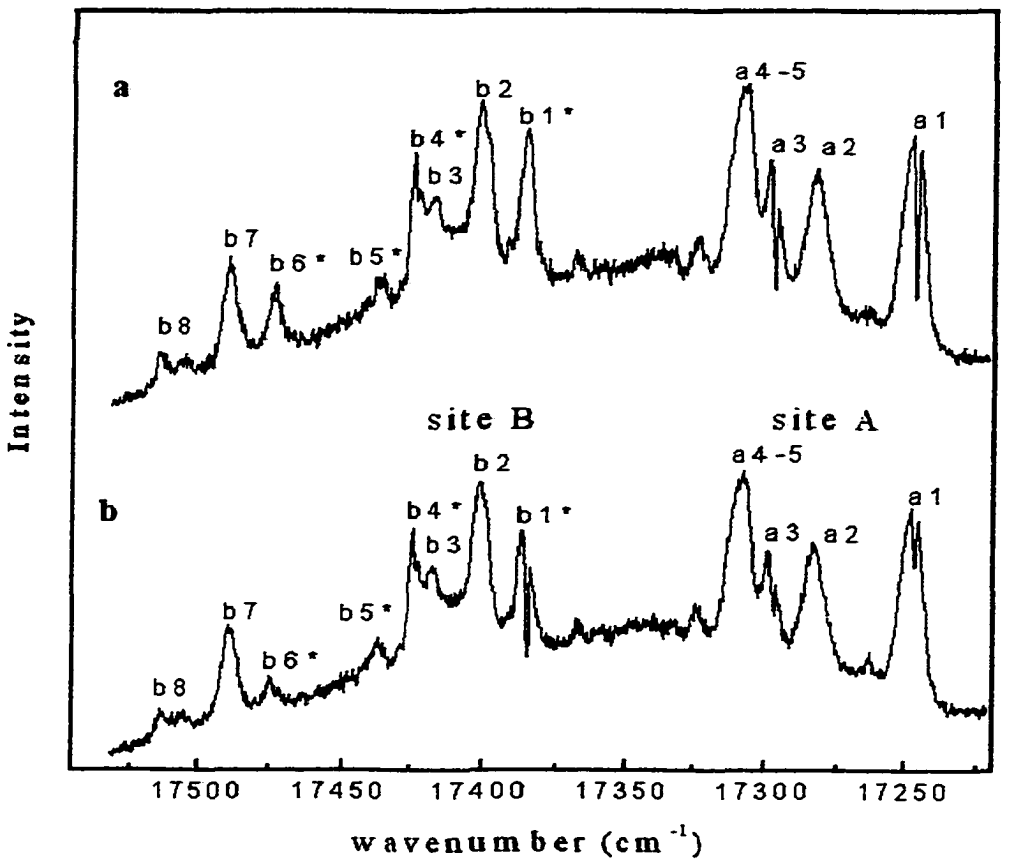


This is evident by the spectral dips in spectral lines a1 and a3 and of the burning down of line b8. Figure 3(b) illustrates the "filling" in of these holes after burning spectral line b1*. The spectral lines that have this unique ability are given in Table 3.3.

**Table 3.3.** Summary of hole burning relationships for lines of site A and B.

| Peaks burned in site B | Lines that increased in intensity in site A |
|---|---|
| b1*, b4* | a1, a4-5 |
| b2, b7 | a1, a3, a4-5 |

Site B is further examined by applying an external electric (Stark) field across the $H_2$iBC/Shpol'skii system while scanning the dye laser. The result of the Stark effect is an overall reduction in intensity of all starred lines in site B with a concomitant increase in intensity of unstarred lines. Surprisingly, line b8 also decreases in intensity upon experiencing the external electric field, which leads to ambiguities as to whether this spectral line is truly a b or b* line. The reduction in intensity of the starred lines only occurs while the electric field is active with the dye laser scanning. Note that after the formation of the starred lines, Stark experiments are performed with no further hole burning in site B. The spectral lines of site A only exhibit minimal Stark broadening.

The spectra indicating the lowering of the overall intensity for the starred lines while experiencing the external electric field are shown in Figures 3.4(a) and (b).

**Fig. 3.4** B site excitation spectrum in absence of applied external electric field (a) and B site excitation spectrum obtained while applying an external electric field of 11.8 kV/cm (b).

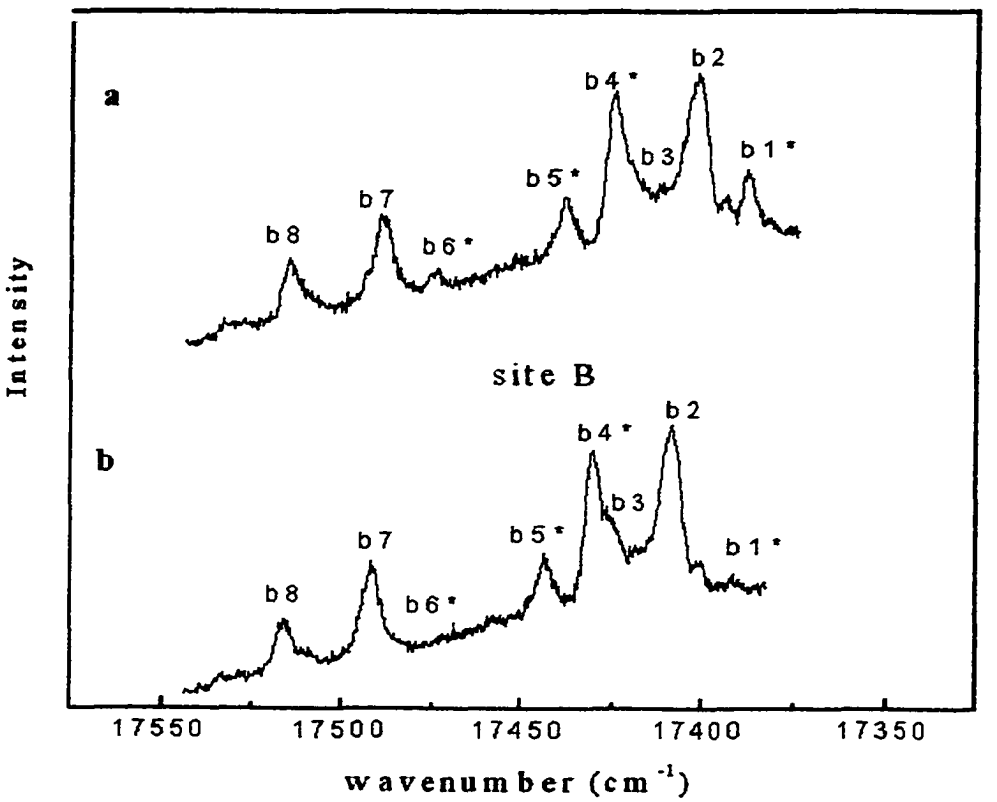


Figure 3.4(a) is a truncated version of site B from the entire excitation spectrum. Figure 3.4(b) is the same truncated spectrum experiencing an electric field of 11.8 kV/cm. Upon comparison, Figure 3.4(b)

displays a drop in spectral intensity for all starred lines in site B. A minimum electric field of 7.87 kV/cm is needed to initiate this effect.

### 3.4 Discussion

Due to molecular similarities in $H_2$iBC and porphyrin, we discuss the orientation of $H_2$iBC in an n-octane matrix with respect to porphyrin. In a Monte Carlo calculation of porphins embedded in an n-octane matrix, Koehler[8] presented evidence that in site A the guest porphin displaces two host n-octane molecules, and the plane of the molecule is positioned in the b-c plane of the crystal (Fig. 3.5). Site B involves displacement of three n-octane molecules , with the molecular plane positioned in the crystal a-c plane (Fig. 3.5).

**Fig. 3.5** Diagram of $H_2$iBC in site A (above) and site B (below). The n-octane crystal is shown in the b-c plane perpendicular to crystal axis a. The c axis is horizontal. The $H_2$iBC molecule is shown in the x-y plane perpendicular to the molecular z-axis. In site B, the n-octane molecule is shown in the a-c plane perpendicular to crystal axis b.

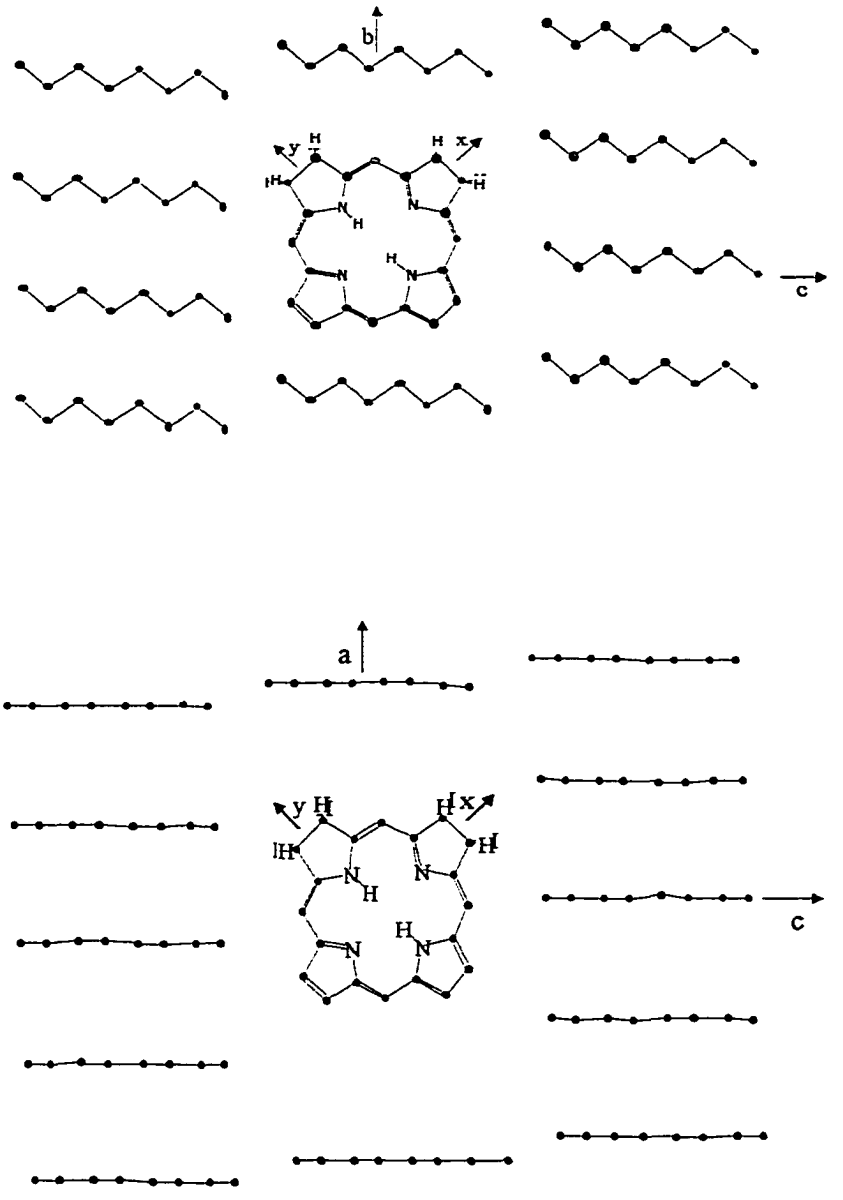

In each of these sites there are four likely minimum orientations of the molecule corresponding to successive rotations by $90^0$ about the z (out of plane) axis. In site A, the appearance of only five lines, one (a2) which does not burn, can be explained if one orientation is sufficiently symmetric that two orientations are identical, resulting in the coincidence of four lines. In site B, the fact that only four lines appear initially indicates that either only two of the orientations are occupied on cooling, with both phototautomers present, or that all four orientations are occupied with only one phototautomer in each orientation. The latter would most likely result in pair-wise burning patterns. However, we observe that burning in any of the initial four lines results in four new lines. This can be explained only if molecules can be photophysically rotated in plane by $90^0$ upon burning. This indicates that only two orientations, with both phototautomers, are initially occupied, and that burning causes tranformation among all eight possible configurations.

Koehler's[8] analysis was based on crystallographic data for n-octane obtained by Mathisen et al.[9] at 90 K. Using these results alone, it is difficult to explain our results upon burning site B. However, recent findings Neumann et al.[10], via neutron diffraction studies,

confirm the n-octane structure obtained by Mathisen et al. for temperatures greater than 55 K, but below this temperature they observed a phase change for the crystal lattice that led to a doubling of the (longitudinal) b axis of the unit cell.[10] The existence of this phase change provides a reasonable explanation for our results. Since the unit cell is doubled along the crystal b axis below 55 K, the molecular environment is somewhat of lower symmetry than above 55 K, allowing for more distinct orientational sites. Furthermore, on burning at these laser powers, some local heating is inevitable, resulting in possible elevation of the local temperature above the phase transition.. This would allow rotation of molecules and most likely reorientation of molecules in site B, which would lead to transformation among the configurations.

The phase change for n-octane, prompted by localized heating during excitation, also explains the ability to burn from lines in site B to lines in site A. During excitation, localized heating causes a softening of the n-octane lattice. The relaxed environment allows for molecules in site B to photophysically transform into lines of site A, even with the sites being perpendicular in the n-octane lattice.

References-Chapter 3

1. Huang, W. Y.; Wild, U. P.; Johnson, L. W. J. Phys. Chem. **96**, 6189 (1992).

2. Johnson, L. W., Murphy M. D., Pope C., Foresti M., and Lombardi, J. R. J. Chem. Phys. **86**, 4335-4340 (1987).

3. Voelker, S., Macfarlane R. M., Genack, A. Z., and Trommsdorff, H. P. J. Chem. Phys. **67**, 1759-1765 (1977).

4. Voelker, S., and Macfarlane, R. M. Chem. Phys. Lett. **61**, 421-4 25 (1987).

5. Voelker, S., and van der Waals, J. H. Molecular Physics. **32**, 1703-1718 (1976).

6. Jansen, G., Noort, M., van Dijk, N., and van der Waals, J. H. Molecular Physics. **39**, 865-880 (1977).

7. Egorova, G. D.; Solov'ev, K. N.; and Shulga, A. M. Zh. Obshch. Khim. **37**, 357 (1976).

8. Koehler, T. R. J. Chem. Phys. **72**, 3389 (1980).

9. Mathisen, H.; Norman, N.; Pedersen, B. F. Acta Chem. Scand. **21**, 127-135 (1967).

10. Neumann, M. A.; Johnson, M. R.; Radaelli, P. G. to be published.

# Resonance Raman Spectroscopy of Mass Selected $Al_2$ in an Argon Matrix

Chapter 4

## 4.1 Introduction

In previous years there has been confusion as to the quantum designation of the ground state of $Al_2$. This was due to the various electronic configurations available for the ground state via $\sigma\sigma$, $\sigma\pi$, or $\pi\pi$ chemical bonding. Sound evidence was presented by Cai, Dzugan, and Bondybey[1], via fluorescence studies of laser vaporized aluminum, and Fu, Lemire, Bishea, and Morse[2], via resonant two photon ionization of jet cooled aluminum dimers, that the ground state for $Al_2$ is of $^3\Pi_u$ symmetry. Cai et al.[1] also reported a ground state frequency of 284.2 $cm^{-1}$ for aluminum dimer.

In this paper we present the resonance Raman spectrum of aluminum dimers in an argon matrix. Exciting with various lines of the visible, and near infrared spectral regions, we obtain a fundamental at 292.3 (5) $cm^{-1}$. This is accompanied by a progression of lines up to 1149 (1) $cm^{-1}$. The spectroscopic constants for the aluminum dimer were obtained by extrapolating successive differences of band centers of the resonance Raman spectrum of the dimer. This leads to a ground state vibration of $\omega_e$ = 295.7 (5) $cm^{-1}$, with an anharmonicity of $\omega_e x_e$ = 1.68 (5) $cm^{-1}$. Our results are in

agreement with the work of Cai et al. and Fu et al. and we add confirmation that the ground state of $Al_2$ is $^3\Pi_u$.

## 4.2 Experimental

The resonance Raman spectrum of $Al_2$ was acquired using the CCNY Metal Cluster Deposition Source (Fig 4.1). The design of this apparatus has been discussed in detail in other publications[3,4] but will be mentioned briefly here for the resonance Raman experimentation of $Al_2$. An argon ion beam of 10 mA (at 25 eV) sputters a water cooled aluminum metal target, purchased from Alfa Aesar at 99.9% (REO). A series of einzel lenses collect the sputtered aluminum cluster ions from the metal sputtering region. A Wien filter mass selects the focussed aluminum cluster ions. Any neutral aluminum atoms produced during the sputtering process that pass through the mass selector are removed via a $10^0$ bend in the path following the Wien filter. A second set of einzel lenses focus the mass selected aluminum dimer cations into the deposition region, which are then codeposited with electrons, for neutralization, onto a $CaF_2$ substrate. A cryostat pumps the deposition region to cool the surface of the substrate to ~ 16 K. To prevent degradation of the aluminum dimers

**Fig. 4.1** Picture of the CCNY Metal Clusters Beam (above) and overhead schematic of the apparatus (below).

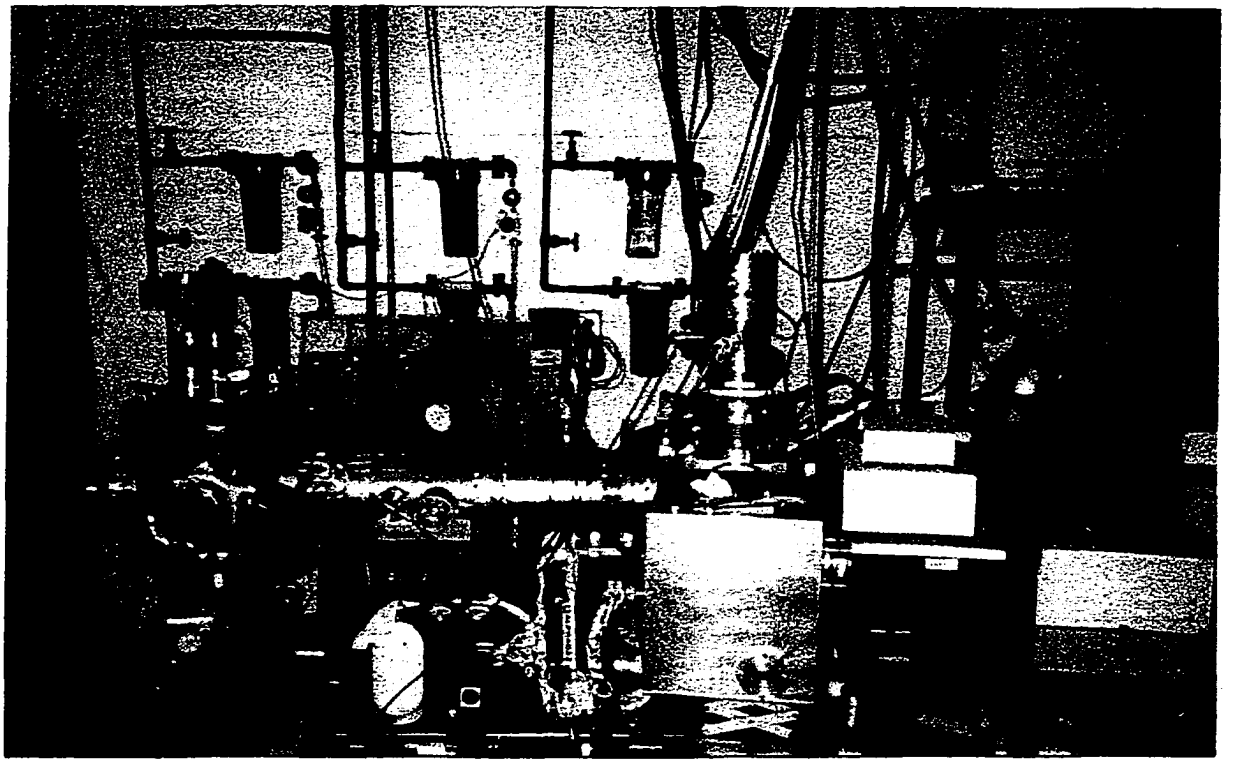

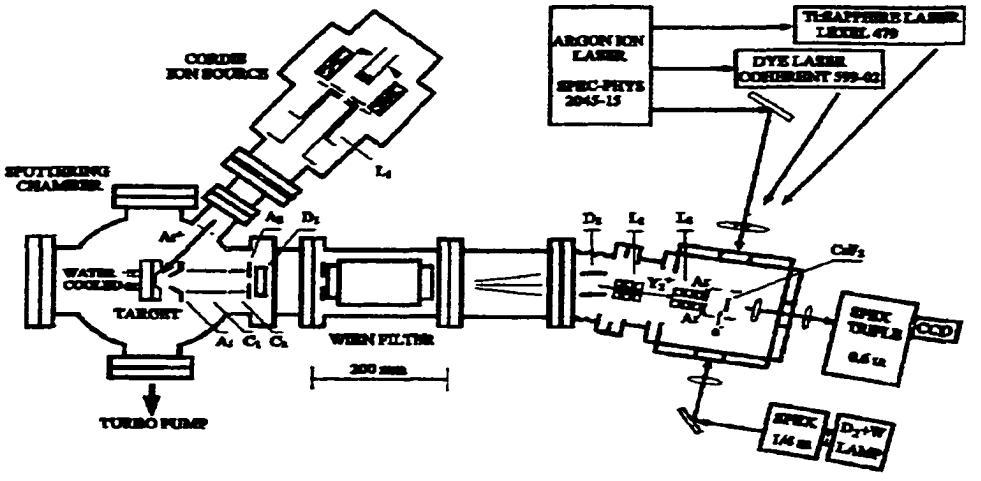

upon impact with the $CaF_2$ substrate, $Al_2$ clusters are slowed to ~ 15 eV to ensure a soft landing on the substrate. The current under hard landing conditions was measured at 60 nA. The $Al_2$/Ar matrix had a growth rate of ~ 6μm/h. The argon:metal ratio was ~ $10^4$:1. A resonance Raman spectrum was recorded after a six hour deposition at a current of ~ 50 nA for $Al_2$.

The resonance Raman spectroscopy was carried out *in situ* on the matrix sample. An absorption spectrum, in the form of a "scattering depletion spectrum" (SDS) was also obtained. The "SDS" absorption is a ratio between scattered light from the edge and center, where most of the sample is deposited. The scattered light is collected at a $90^0$ angle from the incident radiation. The absorption spectrum was recorded after a six hour deposition at a current of ~ 50 nA for $Al_2$. No obvious absorption band could be assigned to $Al_2$.

The visible lines of a Spectra Physics 2045 argon ion laser, laser lines from a Coherent model CR599 dye laser, employing the dyes R6G, R110, and DCM, and near IR lines from a Lexel model 479 titanium sapphire laser were used to observe resonance Raman features of the mass selected aluminum dimers. The 327.0 $cm^{-1}$ line of the $CaF_2$ substrate was used to calibrate all Raman shifts. The

Raman excitation profile for $Al_2$ was generated by stepping the dye laser in increments of ~ 4 nm and observing the varying intensities of the Raman spectrum. The detection system for the metal cluster beam consists of a Spex 1877E 0.6m Triplemate Spectrometer coupled with a liquid nitrogen cooled CCD system (Spectrum One and CCD30).

## 4.3 Results

The resonance Raman spectrum of $Al_2$ in an argon matrix is shown in Fig. 4.2. These bands are observed by probing the $Al_2$/Ar matrix with excitation frequencies that range from 620 to 760 nm. At an exciting wavelength of 660 nm, a total of nine bands were observed for the dimer ranging from 278 $cm^{-1}$ to 1149 (1) $cm^{-1}$. Through temperature annealing of the resonance Raman spectrum $Al_2$ from 16 K to 38 K, it was concluded that the 278 and the 285 (5) $cm^{-1}$ lines are side bands associated with the 292.3 $cm^{-1}$ line arising from site effects of the Ar matrix. We assign the 292.3 (5) $cm^{-1}$ line to the ground state vibration for aluminum dimer. This Raman line gives a progression up to 1149 $cm^{-1}$. Significant resonant Raman enhancements of the 292.3 $cm^{-1}$ line, in a spectral range of 660 nm to

**Fig. 4.2** Resonance Raman spectrum of $Al_2$ in argon matrices excited at 660 nm.

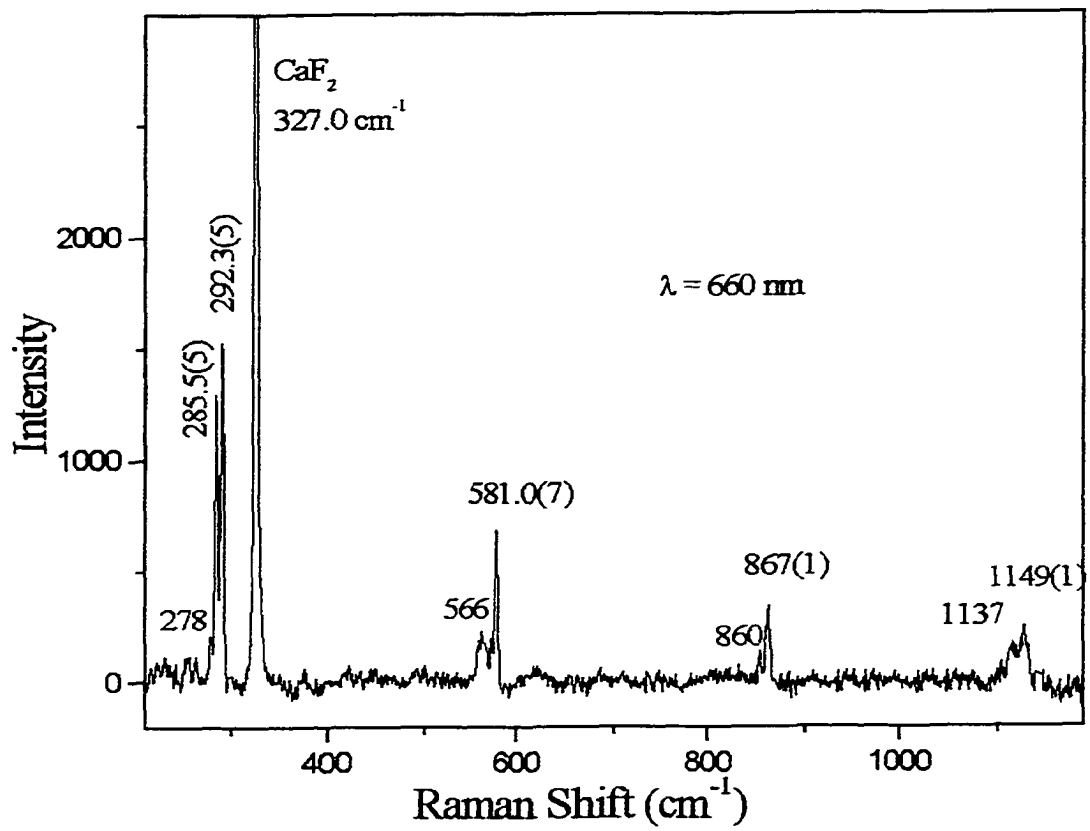

730 nm ( Fig. 4.3), further confirms our designation of this line as the ground vibration. This band corresponds to the absorption observed by Douglas, Hauge, and Margrave[6] at 699 nm. Taking successive differences of band centers in the spectrum, we obtain, using a least squares fit, $\omega_e = 295.7\ (5)\ cm^{-1}$ and $\omega_e x_e = 1.68\ (8)\ cm^{-1}$.

**Fig. 4.3** Resonance Raman excitation profile of line 292.3 and 285.5 $cm^{-1}$. Note that the 292.3 $cm^{-1}$ line shows significant resonant enhancement

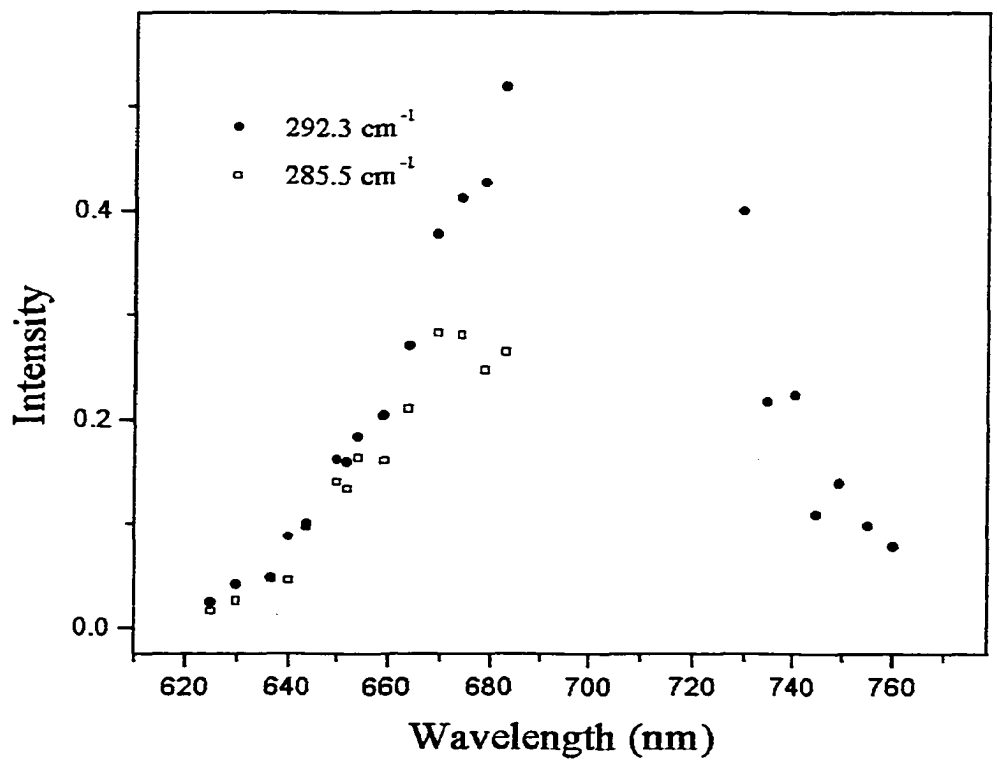

## 4.4 Discussion

In earlier work on $Al_2$, there were ambiguities as to the designation of the ground state for aluminum dimer. The confusion for this assignment is due to the several electronic configurations $Al_2$ can attain by placing two 3p electrons in either a $\sigma_g$ or $\pi_u$ bonding orbital. With this, there are three reasonable designations for the ground state of $Al_2$, a $^1\Sigma_g^+$ state from the $\sigma_g^2$ configuration, a $^3\Pi_u$ from the $\sigma_g^1\pi_u^1$ configuration, and a $^3\Sigma_g^-$ from the $\pi_u^2$ configuration.[2]

Previous gas phase work on $Al_2$ by Ginter et al.[5], using vaporization of aluminum metal in a graphite tube resistance furnace, gave rotational spectra that displayed a 7:5 ratio of alternating intensities of the spectral branches. This pattern is characteristic of a homonuclear diatomic molecule with a nuclear spin of I = 5/2. With their spectral observations and through interpretation of the rotational bands, Ginter et al. reasoned that the only allowable electronic transitions for $Al_2$ were of the $^3\Sigma_u^- \leftarrow {}^3\Sigma_g^-$ and $^3\Sigma_g^+ \leftarrow {}^3\Sigma_u^+$ type.[5] Douglas et al.[6], in their observation and spectral interpretation of absorption characteristics of $Al_2$ isolated in a krypton matrix, designated the ground state symmetry for aluminum dimer as a $^1\Sigma_g^+$.

Not until the work of Cai, Dzugan and Bondebey[1] and Fu, Lemire, Bishea, and Morse[2] was this problem resolved. Using fluorescence studies of laser vaporized aluminum, in a spectral range of 27,000 to 29,000 $cm^{-1}$, Cai et al.[1] observed vibronic bands in the form of triplets with unequal intensities and a constant spacing of ~ 32 $cm^{-1}$. They observed a ground state vibration of 284.2 $cm^{-1}$. The unequal intensities observed in the triplet bands were attributed to thermal populations of the spin-orbit components in the lower state.[1] Their experimental observations were taken as evidence for $^3\Pi_u$ as the ground state.

Through resonant two-photon ionization (R2PI) of jet cooled $Al_2$ molecules, Fu et al.[2] also concluded that the ground state was unequivocally of $^3\Pi_u$ symmetry. Their R2PI rotational spectrum lacked the 7:5 intensity alternation of the spectral bands common for a $^1\Sigma \leftarrow {}^1\Sigma$ homonuclear diatomic transition with nuclear spin I = 5/2. This led to their reasoning that the $Al_2$ electronic transition was of the $\Omega' = 0 \leftarrow \Omega'' = 0$ type, therefore eliminating the $^1\Sigma_g^+$ as the ground state.[2] The $^3\Sigma_g^-$ state was eliminated as a possibility for the ground state due to their observation of multiplet splittings of the upper states of the E, E″, F′, and F band systems of their rotational spectra.[2]

Resolvable Λ doublets were observed, which imply the originating state has a triplet or higher multiplicity.[2] Of the three symmetries, $^1\Sigma_g^+$, $^3\Pi_u$, and $^3\Sigma_g^-$, only the $^3\Pi_u$ state fulfills this requirement. They obtained $\omega_e = 285.8$ cm$^{-1}$ for the ground state.

Since our observations are made at 16 K, the electronic transitions must originate from the ground state. We take our value of $\omega_e$ to display a reasonable matrix shift from the gas phase result obtained for the $^3\Pi_u$ state (as opposed to the value of 350 cm$^{-1}$ for the $^3\Sigma_g^-$ state).[5] Our results therefore add confirmation to the assignment of the $^3\Pi_u$ as the ground state.

**References-Chapter 4**


1. Cai, M. F.; Dzugan, T. P.; Bondybey, V. E. Chem. Phys. Lett. **155**, 430-436 (1989).

2. Fu, Z.; Lemire, G. W.; Bishea, G. A.; Morse, M. D. J. Chem. Phys. **93**, 8420-8441(1990).

3. Hu, Z.; Shen, B.; Deosaran, S.; Lombardi, J.; Lindsay, D. M.; Harbich, W. Proc SPIE. **65**, 1559 (1991).

4. Hu, Z.; Shen, B.; Lombardi, J.; Lindsay, D. M. J. Chem. Phys. **96**, 8757 (1992).

5. Ginter, D. S.; Ginter, M. L.; Innes, K. K. Astrophys. J. **139**, 365 (1963).

6. Douglas, M. A.; Hauge, R. H.; Margrave, J. L. J. Phys. Chem. **87**, 2945 (1983).

# Resonance Raman and Fluorescence Spectra of Mass Selected Molybdenum Dimer and Trimer in Argon Matrices

## Chapter 5

## 5.1 Introduction

There has been considerable interest in molybdenum compounds due in part to their importance in environmental systems, the human body, catalysis, and other areas.[1] It is therefore of interest to consider molybdenum in its bare metal cluster form. Molybdenum dimer, $Mo_2$, is noted for having one of the strongest metal-metal bonds with a likely bond order greater than four,[2,3] and it would be worth while to examine whether this strong bonding extends to the trimer.

For $Mo_2$, much spectroscopic interest has been centered on characterization of its optical properties. Efremov et al. detected vibrational and rotational frequencies due to $Mo_2$ produced via flash photolysis of crystallized molybdenum hexacarbonly.[4] They probed the gaseous $Mo_2$ molecules observing three optical transitions which they designated system A, system B, and system C. They found vibrational fundamentals in each of the states involved, from which they obtained the lowest state fundamental as $\omega_e = 477\ cm^{-1}$.[4]

Pellin et al., via pulsed laser probing of $Mo_2$ in an argon matrix, observed fluorescence in the spectral range of ~ 724-850 nm when exciting at various wavelengths ranging from 498-543 nm.[5] Their

fluorescence spectra yielded two sets of nearly identical progressions that are slightly shifted in spectral range from one another. These were attributed to the existence of two sites in the argon matrix into which $Mo_2$ can be incorporated.[5] Because of this, they termed the emission as red and blue emission. From their fluorescence results, Pellin et al. determined the vibrational frequency of a low lying state, presumed to be the ground state, with $\omega_e$ = 473 $cm^{-1}$ for the red emission and $\omega_e$ = 477 $cm^{-1}$ for the blue emission.[5] This was confirmed by observation of a single Raman line at 475 $cm^{-1}$ in a narrow spectral range.[6]

It was also observed by J.B. Hopkins et al. that $Mo_2$ displayed an electronic state with $\omega_e$ = 449 $cm^{-1}$ via pulsed laser vaporization of the metal and forming ultra cold mass selected metal clusters by resonant two photon ionization spectra.[7] The vibrational frequencies for several electronic states of $Mo_2$ obtained by Efremov et al.,[4] Pellin et al.,[5] and J.B. Hopkins et al.[7] were predicted in calculations by Bursten et al.[2] via multiconfigurational SCF with configuration interaction. No previous spectroscopic work has been carried out for $Mo_3$.

In this work we present the resonance Raman spectra, the absorption (scattering depletion) spectra, and the Raman and fluorescence excitation profiles of the mass selected metal clusters of molybdenum dimer and trimer. We observe the resonance Raman spectra of $Mo_2$ in the excitation region of ~ 451-461 nm and at exciting lines of 488 nm, 496.5 nm, and 501.7 nm. The Raman spectrum of $Mo_2$ displays three fundamentals at 394.5 (12) $cm^{-1}$, 446.0 (81) $cm^{-1}$, and 473.3 (15) $cm^{-1}$. The 394.5 $cm^{-1}$ peak is the most intense and includes a series of three overtones up to 1552 $cm^{-1}$. Fluorescence from $Mo_2$ was observed exciting in the region 440-685 nm. The fluorescence in this region is the same as that obtained by Pellin et al.[5] Both blue and red fluorescence of $Mo_2$, due to matrix effects, are observed in our spectrum. We also extended the region of excitation consisting of weak fluorescence peaks to ~ 560-680 nm.

There has been no previous resonance Raman work on molybdenum trimers. The absorption (SDS) spectrum of $Mo_3$ displays a broad band extending from ~ 575-625 nm, with an absorbance maximum around ~ 600nm. We excited near the absorbance maximum and observed four resonance Raman lines attributed to molybdenum trimer. These bands were observed at 224.5

(5) $cm^{-1}$, 236.2 (8) $cm^{-1}$, 386.8 (12) $cm^{-1}$ and 446.9 (7) $cm^{-1}$. We assign the 386.8 $cm^{-1}$ peak as the ground state fundamental of the symmetric stretch $\nu_1(a_1)$. The lines at 236.5 and 224.5 $cm^{-1}$ are attributed to the antisymmetric stretch $\nu_2(b_1)$ and the bend $\nu_3(a_1)$ respectively. The line observed at 446.9 $cm^{-1}$ is assigned as an overtone to the antisymmetric stretch.

## 5.2 Experimental

The instrumentation for the CCNY Metal Cluster Deposition Source has been described in detail in previous publications[8,9] but will be briefly detailed in this experimental section. A 10 mA argon ion beam (at 25 keV) sputters a water cooled molybdenum metal target, purchased from Alfa Aesar at 99.9% purity. Molybdenum cluster ions are collected from the metal sputtering region by a series of einzel lenses. Ions are then mass selected via a Wien filter. The path following the Wien filter is bent by $10^0$ to remove any neutral molybdenum atoms produced during the sputtering process.

Mass selected molybdenum cluster ions are then focused by an einzel lens into the deposition region where $Mo_2^+$, or $Mo_3^+$, is co-deposited with argon gas and electrons for neutralization onto a $CaF_2$

substrate. All this is done while the $CaF_2$ substrate is at a temperature of ~ 16 K. Before depositing the $Mo_2$, or $Mo_3$, onto our substrate, the mass selected ions were slowed to 10 eV for $Mo_2$ and to 24 eV for $Mo_3$ by a Faraday cage surrounding the cooled $CaF_2$ plate. This is done to produce soft landing conditions for the mass selected sample. The currents for hard landing conditions ($V_{dep}$ = 300 V) were measured for $Mo_2^+$ to be 150 nA and 35 nA for $Mo_3^+$. The argon/$Mo_2$($Mo_3$) matrix was grown at ~ 6μm/h with an Ar : metal ratio of ~ $10^4$:1. Upon comparison of atomic molybdenum excitation features with those of $Mo_2$ and $Mo_3$, with molybdenum atoms deposited under the same conditions, the fragmentation ratio for $Mo_2$ is estimated to be ~ 3% and for $Mo_3$ < 1%.

The matrix samples were probed *in situ* via absorption and Raman spectroscopy. The absorption spectrum for both $Mo_2$ and $Mo_3$ were obtained via a scattering depletion spectrum (SDS). With SDS, a ratio between scattered light from the center of the substrate, where most of the sample has been deposited, and scattered light from the edge of the substrate are collected at a $90^0$ angle to the incident. For these experiments, the absorption (SDS) spectrum was recorded after a six hour deposition of ~ 600 nA for $Mo_2$ and ~ 170 nA for $Mo_3$. The

matrix sample was also probed via temperature annealing. The temperature of the sample matrix was raised slowly from 16 K to 38 K and then lowered back to 16 K. Subsequent Raman spectra were taken when the system returned to 16 K. Annealing temperatures were controlled with a Scientific Instrument Series 5500 Temperature Controller.

Raman experiments were carried out using the visible lines of a Spectra Physics 2045 argon ion laser, which pumped a Coherent model CR599 dye laser employing the dyes R6G, Stilbene 3, R110, and DCM. All Raman shifts were calibrated using the 327.0 $cm^{-1}$ line of the $CaF_2$ substrate. Observing the Raman spectra of $Mo_2$ while tuning the dye laser in small increments in various absorption regions for the dimer generated the fluorescence and Raman excitation profiles for $Mo_2$. This method was also used to generate the Raman excitation profile for $Mo_3$. The detection system for our cluster deposition source consists of a Spex 1877E 0.6m Triplemate Spectrometer coupled with a liquid nitrogen cooled CCD system (Spectrum One and CCD30). The information from the CCD is interpreted and displayed by DM3000R software interfaced to a computer.

## 5.3 Results and Discussion: $Mo_2$

The resonance Raman spectrum of an ~ 600 nA-h sample of $Mo_2$ in an argon matrix is shown in Figure 5.1. The Raman spectrum gives three Raman fundamentals at 394.5 $cm^{-1}$, 445.0 $cm^{-1}$, and 473.3 $cm^{-1}$ and three overtones of 394.5 $cm^{-1}$ at 783.0 (52) $cm^{-1}$ and 1167.0 (49) $cm^{-1}$ and 1552 $cm^{-1}$. Normally only a single fundamental is observed for a diatomic molecule unless tied to an origin of a low lying electronic state.[10,11] Surprisingly, we observe several lines with the same origin (i.e. the Rayliegh line). Note, however, that two of these fundamentals (445 and 473 $cm^{-1}$) were previously observed in emission and absorption studies.[4,5] The 394.5 $cm^{-1}$ Raman shift is by far the most intense Raman peak of the three vibrational fundamentals observed in the Raman spectrum of $Mo_2$. Pellin et al.[6] observed only one line at 475 $cm^{-1}$ in a Raman spectrum exciting with several argon ion laser lines. However, the large number of atoms in their sample produces considerable interference from fluorescence, which most likely prevents possible observation of the lower frequency lines. With the mass selection provided in our experiment, this spectral interference is not a problem.

**Fig. 5.1** Resonance Raman spectrum of $Mo_2$ in argon matrices excited at 457.9 nm. The inset shows the significant Raman enhancement of the 394.5 $cm^{-1}$ line.

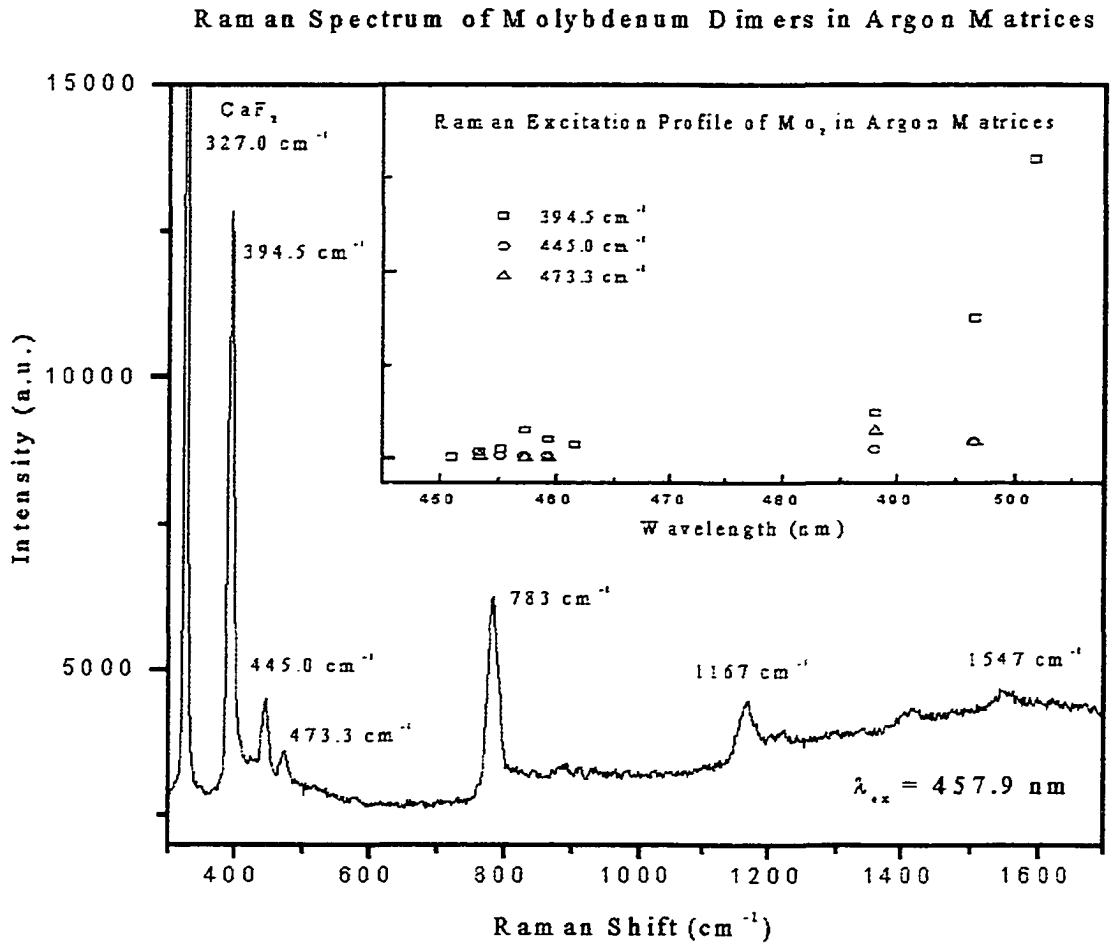

The Raman excitation profile of $Mo_2$ is shown as an inset of Figure 1. One weak absorption region is centered at ~ 457 nm, and the other region is near ~ 500 nm. In the region above 500 nm, fluorescence begins to obscure our Raman excitation profile. Note that the 395 $cm^{-1}$ Raman shift shows a peak at ~ 457 nm and rises in intensity as it approaches the ~ 500 nm region while the profiles arising from the other two lines remain relatively flat. This latter is in agreement with the observation of Pellin et al.[5] for the intensity variation of the 475 $cm^{-1}$ line. It is most likely that the 394.5 $cm^{-1}$ line is resonantly enhanced, while the other two are from normal Raman scattering.

We also observe fluorescence from $Mo_2$ in the exciting region of ~ 520 nm. This fluorescence for $Mo_2$ is identical with that which was observed previously by Pellin et al.[5] We observe, as did they, the red and blue fluorescence shift of the spectral peaks due to the ability of the dimer to be incorporated into two different sites in the argon matrix. We also extended the region of fluorescence excitation for $Mo_2$ into the region between 556 nm to 725 nm (Fig. 5.2). This region displays the same red and blue emission due to site effects of $Mo_2$ that were observed in the fluorescence region at ~ 520 nm.

**Fig. 5.2** Fluorescence excitation profile of $Mo_2$ in argon matrices.

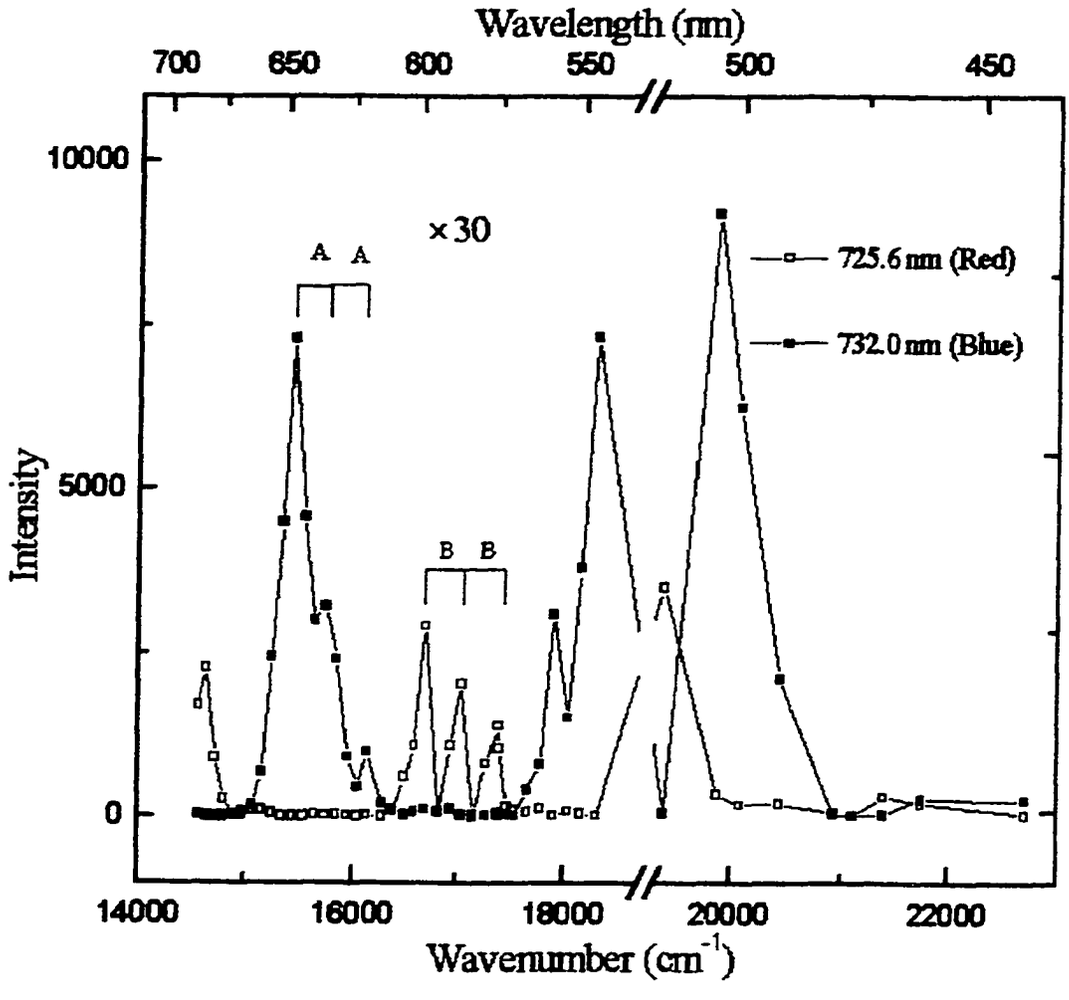

However the fluorescence excitation profile of $Mo_2$ reveals several new optical transitions, marked B, at 16,698 (0-0) $cm^{-1}$, 17,049 (0-1) $cm^{-1}$, and 17,397 (0-2) $cm^{-1}$ for the red site emission, with and average spacing of $\sim 350$ $cm^{-1}$. For the blue site emission these transitions are observed, marked A, at 15,444 (0-0) $cm^{-1}$, 15,744 (0-1) $cm^{-1}$, and 16,123 (0-2) $cm^{-1}$, with and average spacing of $\sim$ 340 $cm^{-1}$. The intensity observed here is much weaker than that observed near 500 nm and therefore presumed to represent nominally forbidden transitions. Upon annealing to 38 K, the blue site fluorescence decreases in intensity while the red site fluorescence increases in intensity. This indicates that the red site is indeed the most stable.

Our observation of the three different fundamentals in the Raman spectrum implies that we are observing spectra in three distinct states and leads us to ask the question, which corresponds to the ground state? Clearly all three can not, and at these temperatures our experiment can only be explained if two of these states are populated by some optical pumping mechanism. From vibrational analysis of the observed emission of $Mo_2$, Efremov et al.[4] obtained $\omega_e$ = 477.1 $cm^{-1}$ for the lowest state, which they designated, $X(^1\Sigma_g^+)$. For the excited states they found $\omega_e = 443.4$ $cm^{-1}$ $A(^1\Sigma_u^+)$, $\omega_e = 412.0$ $cm^{-1}$

$B(^1\Pi_u)$, and $\omega_e = 408.0$ cm$^{-1}$ $C(^1\Sigma_u^+)$.[4] Agreement of $\Delta G''_{v+½}$ values for the B and C systems indicates that they both have a common lower state.[4] Furthermore, they reasoned that since the absorption frequencies of the A and C systems correspond to bands observed in an argon matrix,[4] which implies that the lower state in each of these systems must be the ground state.

However, our observation that the 394.5 cm$^{-1}$ line is resonantly enhanced in the region near 500 nm (inset of Fig. 5.1), while the lines at 446.0 cm$^{-1}$ and 473.3 cm$^{-1}$ apparently are not, calls this into question. The observed resonance enhancement of the 395.4 cm$^{-1}$ line implies either that it is the vibrational frequency of the ground state, or both the ground state (presumably with $\omega_e = 473$ cm$^{-1}$) and the electronic state with $\omega_e = 394.5$ cm$^{-1}$ both have optical transitions near 500 nm.

Further evidence comes from the observation of the power dependence of the ratio of intensities of the 394.5 cm$^{-1}$ line to that of the 473 cm$^{-1}$ line (Fig 5.3). This is shown in Figure 3 over a laser power range of 25-100 mW. Although the point obtained at the lowest power is relatively unreliable, the trend is clear. As the power is increased, the relative population of the state associated with the

**Fig 5.3** Laser power dependence ratio of Raman lines 395 and 473 $cm^{-1}$.

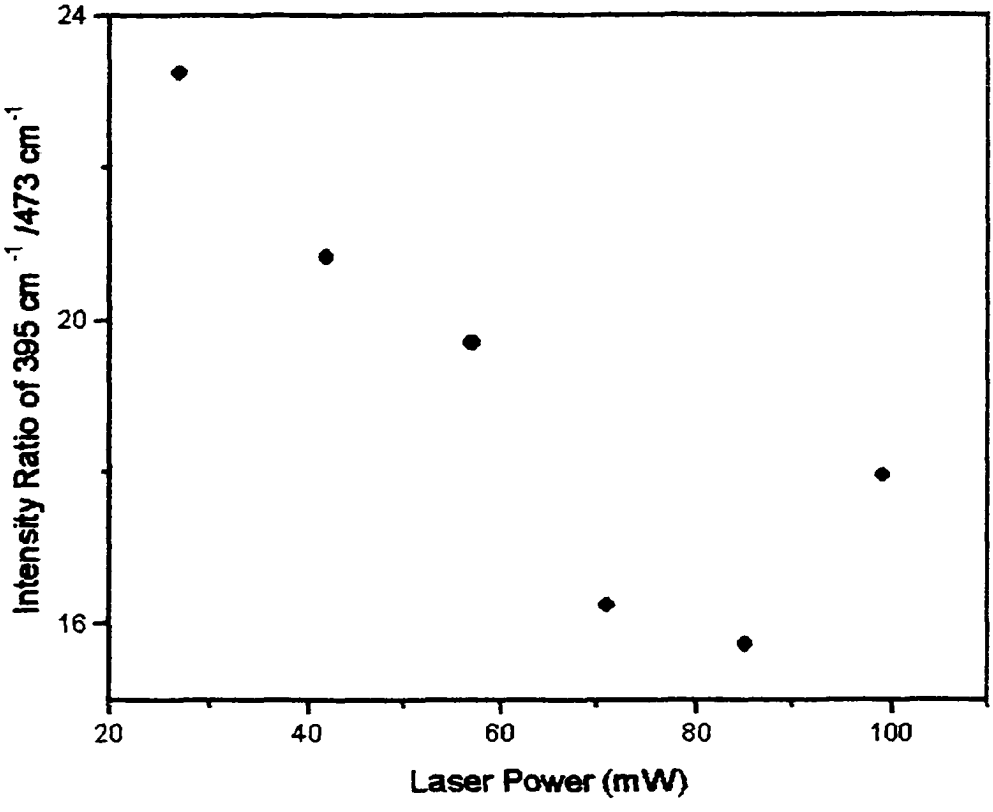

394.5 $cm^{-1}$ line decreases with respect to that of population of the state corresponding with the 473 $cm^{-1}$ line. A similar trend is observed with the ratio of the 394.5 $cm^{-1}$ to that of the 446 $cm^{-1}$ line. This implies that optical pumping tends to populate the states with frequencies of 446 $cm^{-1}$ and 473 $cm^{-1}$.

These results raise the possibility that all the previous experiments may not be observing the ground state but instead states involving a manifold with a metastable lowest level. Efremov's experiments involve production of $Mo_2$ by flash photolysis, which could easily lead to population of a metastable level. In fact, their maximum intensity was obtained only after a 60 μs delay. The long lived emission observed by Pellin et al.[5] and Heimbrook et al.[12] (> 2 ms) indicates only an emission from a different manifold to a lower state. Note, as pointed out by Simard et al.[13], the lowest energy separated atomic limit ($^7S_3 + {}^7S_3$) gives rise to 7 Hunds case (a) states (of Σ symmetry with spin degeneracies of 1, 3, 5, .....13) or 28 case (c) states. All calculations agree that the ground state must be a $^1\Sigma_g^+$.

There have been several calculations of the ground state frequency. Atha, Hiller, and Guest[3], using single determintal doubly excited CI treatment, indicate $\omega_e$ = 388 $cm^{-1}$. Bursten, Cotton, and

Hall[2] use a multiconfigurational calculation with 3,212 spin adapted configurations. The two calculations differ by the number of bond centered functions and give $\omega_e = 392$ cm$^{-1}$ and 475 cm$^{-1}$ respectively. Despite their observation that increasing the number of configurations tends to decrease $\omega_e$, they choose the higher number as correct since that was more in agreement with the experiments known to them ( i.e. Efremov's). Their lower number, however, is closer to our observed line at 394.5 cm$^{-1}$.

We feel that the evidence presented here raises the possibility the $X^1\Sigma_g^+$ ground state of $Mo_2$ has a vibrational frequency of 394.5 cm$^{-1}$, as observed in our Raman experiments. Also note that it is possible for the states with frequencies of 446 cm$^{-1}$ and 473 cm$^{-1}$ to represent levels in other manifolds that are metastable with respect to the ground state. If correct, our value of $k_e = 4.48$ mdyne/Å, though still very high, indicates a considerably lower bond order for $Mo_2$ than had previously been considered, $ke = 6.43$ mdyne/Å (for $\omega_e = 477$ cm$^{-1}$). Clearly additional experiments are needed to arrive at a definite assignment for molybdenum dimer.

## 5.4 Results and Discussion: $Mo_3$

The absorption spectrum of an ~ 220 nA-h sample of $Mo_3$ in an argon matrix is shown as a "SDS" spectrum in the inset of Figure 5.5. Note, that the Raman excitation profile for $Mo_3$, also shown in the inset of Figure 5.5, mirrors that of the absorption "SDS" spectrum and confirms its assignment to the trimer. The absorption of $Mo_3$ displays a broad band in the region of ~ 575 to 625 nm. The maximum for this absorption is in the region of ~ 600 nm. We excited at 590 nm and observed resonance Raman lines for $Mo_3$ at 224.5 (5) $cm^{-1}$, 236.2 (8) $cm^{-1}$, 386.8 (12) $cm^{-1}$, and 446.9 (7) $cm^{-1}$ (Figure 5.5). We assign the band 386.8 $cm^{-1}$ to the totally symmetric stretch $\nu_1(a_1)$ of triatomic molybdenum ($C_{2v}$). The vibrations at 236.2 and 225.5 $cm^{-1}$ may be assigned to the $\nu_2(b_1)$ antisymmetric stretch and the $\nu_3(a_1)$ bend respectively. The band observed at $\omega_e = 446.9$ $cm^{-1}$ is assigned as an overtone $2\nu_2(a_1)$.

**Fig. 5.6** Resonance Raman spectrum of $Mo_3$ in argon matrices excited at 590 nm. Shown as an inset is the absorption (SDS) spectrum and the Raman enhancement profile of line 224.5 $cm^{-1}$.

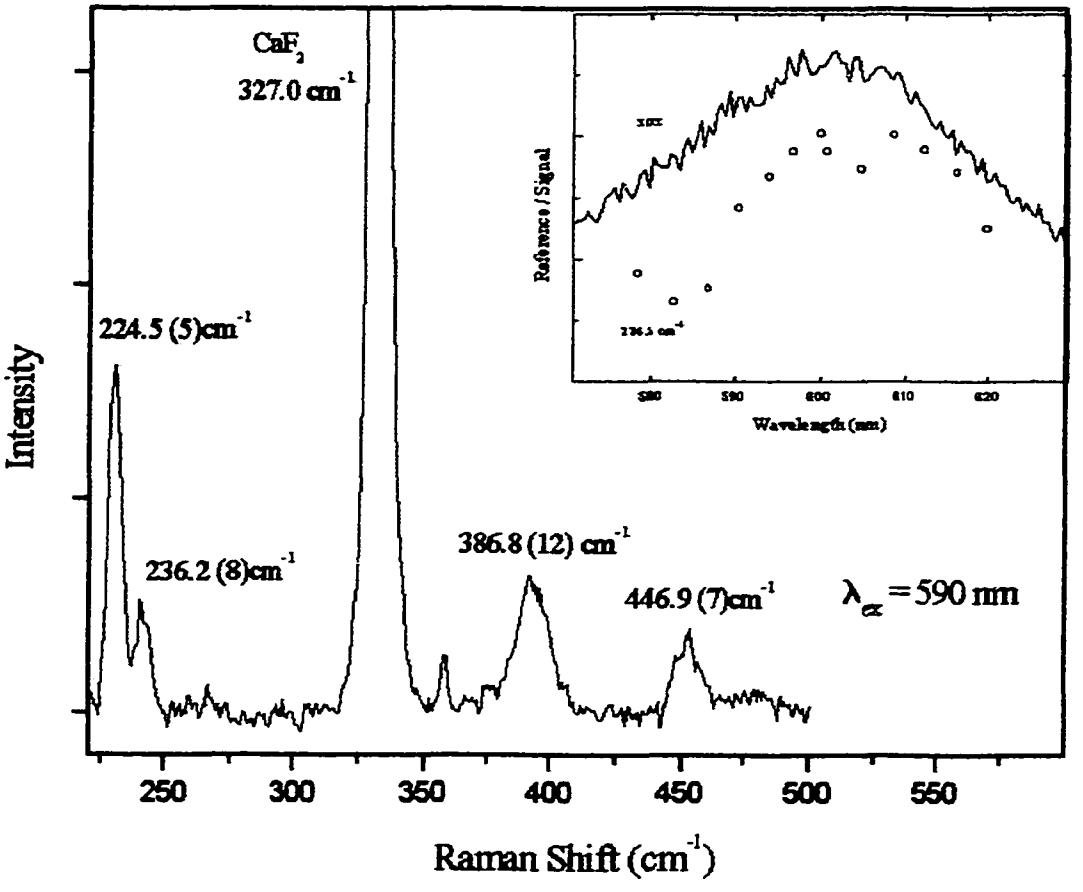

In a recent density functional study of small Mo clusters Pis Diez[16] predicted that the ground state of $Mo_3$ will be an equilateral triangle with a $^3A'_2$ state arising from a $1a'_1{}^2\ 1a''_2{}^2\ 1e'^4\ 2a'_1{}^2\ 3a'_1{}^2\ 1e''^2\ 2e'^2$ configuration. The vibrational frequencies for this state are 271 $cm^{-1}$ (e') and 446 $cm^{-1}$ ($a_1{}^1$), both somewhat larger than the assignments in this study. It might be tempting to assign our observed line at 446.9 $cm^{-1}$ to the symmetric stretch in agreement with the calculation, but then it would be impossible to assign the remaining three lines to a trimer, since only three fundamentals are expected.

The symmetric stretch force constant obtained in the vibrational assignment is $k_e$ = 2.87 mdyne/Å. As suggested by Ozin and Macintosh, the force constant for the trimer should be ~ 1/2 that of the dimer ($k_e$ = 4.48 mdyne/Å)for an equilateral triangle, and ~ 2/3 that of the dimer for linear geometry. Our observed force constant lies between those two limits, consistent with our $C_{2v}$ geometry. Using the central force approximation we obtain an apex angle of $83.7^0$ for the $C_{2v}$ geometry of the trimer.

**References-Chapter 5**


1. Parker, G. A. *Analytical Chemistry of Molybdenum*. Springer-Verlag: New York (1983).

2. Bursten B. E.; Cotton F. A.; Hall, M. B. J. Am. Chem. Soc. **102**, 6348-6349 (1980).

3. Atha, P. M.; Hiller I. H.; Guest M. F. Chem. Phys. Lett. **75**, 84-86 (1980).

4. Efremov, Y. M.; Samoilova, A. N.; Kozhukhovsky V. B.; Gurvich, L. V. V. J. Mol. Spectrosc. **73**, 430-440 (1978).

5. Pellin, M. J.; Foosnaes, T.; Gruen, D. M. J. Chem. Phys. **74**, 5547-5557 (1981).

6. Pellin, M. J.; Foosnaes, T.; Gruen, D. M. *ACS Symposium Series.* **179**, American Chemical Society: Washington, D. C. (1982).

7. Hopkins, J. B.; Langridge-Smith, P. R. R.; Morse M. D.; Smalley, R. E. J. Chem. Phys. **78**, 1627-1637 (1983).

8. Hu, Z.; Shen, B.; Deosaran, S.; Lombardi, J. R.; Lindsay, D. M.; Harbich, W. Proc. SPIE. **65**, 1559 (1991).

9. Hu, Z.; Shen, B.; Lombardi, J. R.; Lindsay, D. M. J. Chem. Phys. **96**, 8757 (1992).

10. Huaiming, W.; Zhendong, H.; Haouari, H.; Craig, R.; Liu, Y.; Lombardi, J. R.; Lindsay, D. M. J. Chem. Phys. **106**, 8339-8343 (1997).

11. Fang, L.; Shen, X.; Chen, X.; Lombardi, J. R. J. Chem. Phys. **113**, 7178-7181 (2000).

12. Heimbrook, L. A.; Rasanen, M.; Bondybey, V. E. J. Phys. Chem. **91**, 2468-2474 (1987).

13. Simard, B.; Lebeault-Dorget, M. A. ; Marijnissen, A.; ter Meulen, J. J. J. Chem. Phys. **108**, 9668-9674 (1998).

14. Lian, L.; Mitchell, S. A.; Rayner D. M. J. Chem. Phys. **98**, 11637-11647 (1994).

15. Ozin, G. A.; McIntosh, D. F. J. Phys. Chem. **90**, 5756 (1986).

16. Diez, R. P. International Journal of Quantum Chemistry. **76**, 105 (2000).

# Resonance Raman Spectroscopy of Mass Selected Chromium Trimers in an Argon Matrix

## Chapter 6

## 6.1 Introduction

This work is an extension of our previous studies on transition metal trimers[1]. Cr is of special interest due to the great disparity between the relatively close d-orbitals and the diffuse nature of the s orbital. The ground state configuration of Cr atom is $3d^5 4s^1$, which provides ample opportunity for multiple bonding, and increasing sophistication of our ability to carry out accurate calculations on these species encourages us to obtain accurate spectroscopic properties.

Transition metal clusters present experimental problems in that it is often difficult to obtain a sample of a particularly chosen cluster, free of contamination from other clusters of nearby nuclearity. Spectroscopic studies of such samples often lead to uncertainty as to the exact nature of the observed species. We have solved this problem by construction of our mass-selection apparatus, which has provided unambiguous spectroscopic results.

In this work we obtain the absorption, and resonance Raman spectrum of mass-selected chromium trimers. The Raman spectrum consists of five lines, four of which form a progression that can be assigned to the symmetric stretch normal mode vibration. The

remaining line can be assigned to the degenerate bend of an equilateral triangle ($D_{3h}$).

## 6.2 Experimental

Previous publications have described in great detail the instrumental setup of the CCNY metal cluster beam.[2,3] In this section we present a brief description of the experimental parameters employed by the apparatus for the formation, mass selection, deposition, and subsequent *in situ* resonance Raman spectroscopy of chromium trimers in an argon matrix. Chromium cluster cations are formed via argon ion plasma bombardment (at ~ 10 mA and accelerated at 25 keV) of a water-cooled chromium metal target (at 300 V) purchased from Goodfellow at 99.7% purity. A series of einzel lenses collect the chromium cluster ions from the sputtering region and focus the ions into the mass selection apparatus. Chromium trimers are then mass selected by a Wien filter. Most neutral chromium atoms produced during the sputtering process that traverse the Wien filter are lost to the system via a $10^0$ bend of the path following mass selection.

Another set of einzel lenses focus the mass selected chromium trimer cations into the deposition region, where they are co-deposited with argon and electrons, for neutralization, onto a $CaF_2$ substrate. The $Cr_3$/Ar matrix is formed under cryogenic conditions (~16 K). Before actual deposition of $Cr_3$ onto the $CaF_2$ substrate, the trimers are slowed to ~ 10 eV, with respect to the potential across the metal target, by a Faraday cage encompassing the cooled $CaF_2$ substrate. This is done to ensure a soft landing of the mass selected sample onto the $CaF_2$ substrate. The current under hard landing conditions was measured to be 40 nA.

The chromium trimers were probed *in situ* via resonance Raman and absorption spectroscopy. The absorption spectrum for $Cr_3$ is obtained using scattering depletion spectrum (SDS). SDS is an absorption measuring technique in which a ratio between scattered light from the center of the $CaF_2$ substrate, where a majority of the sample is deposited, and scattered light from the edge of the substrate is obtained $90^0$ from the incident radiation. The absorption spectrum (SDS) of chromium trimer in an argon matrix was acquired after a five hour deposition of the molecule at an average current of 24 nA,

giving a total concentration of ~ 120 nA-h. As a check on our results, we separately deposited $Cr_2$ with a total concentration of 100 nA-h.

Although a distinct SDS spectrum of $Cr_2$ was obtained, no Raman intensity was observed. Consequently, we could not estimate the fragmentation ratio of $Cr_3$ to $Cr_2$ in the usual fashion. Crude estimates from the SDS spectra give a maximum fragmentation ratio of 10%.

Resonance Raman experiments were performed employing the visible lines of a Spectra Physics 2045 argon ion laser, as well as dye lasers utilizing R6G (spectral range ~ 575 to 622 nm), and DCM (spectral range ~ 630 to 685 nm) dyes. All Raman lines were detected with a Spex 1877E 0.6m Triplemate Spectrometer coupled to a liquid nitrogen cooled CCD (Spectrum One and CCD30). All collected data was interpreted and displayed by DM3000R software interfaced with a computer.

## 6.3 Results

The resonance Raman spectrum of chromium trimer ($Cr_3$) isolated in an argon matrix at ~ 16 K is shown in Fig.6.1. All observed Raman frequencies were averaged over a maximum of 25 spectra in an exciting range of ~ 460 to 685 nm and are calibrated

with respect to the 327 $cm^{-1}$ Raman shift of the $CaF_2$ substrate. At an excitation wavelength of 476.5 nm, the isolated $Cr_3$ displays five distinct Raman lines. The observed frequencies of these lines are 302.0 (87), 400.0 (7), 766.1 (8), 1,100.8 (10), and 1,438.7 (16) $cm^{-1}$. No other lines were observed down to 100 $cm^{-1}$. The Raman line located at 400.0 $cm^{-1}$ is the most intense of all the observable bands in our spectrum and we attribute the three Raman lines at higher

**Fig. 6.1** Resonance Raman spectrum of $Cr_3$ in argon matrices excited at 476.5 nm.

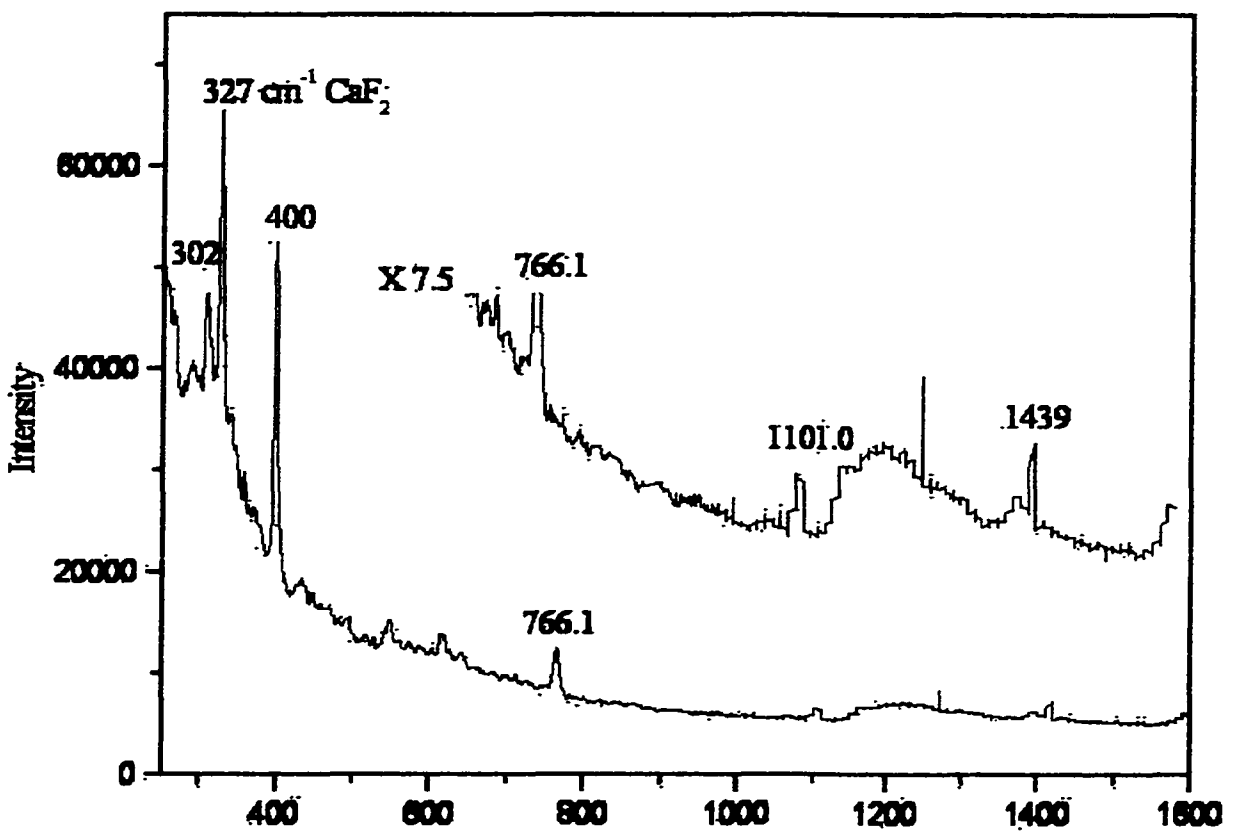

frequencies, up to 1,438.7 $cm^{-1}$, as a spectral progression in the 400.0 $cm^{-1}$ frequency. We assign the 400.0 $cm^{-1}$ line to the totally symmetric stretch $\nu_1(a'_1)$ of chromium trimer.

Taking successive differences of Raman band centers and employing a least squares fit (we have left out the line at 1,438.7 $cm^{-1}$ from this analysis, due to low signal-to-noise ratios), we obtain a ground state harmonic frequency of $\omega_e$ = 432.2 (16) $cm^{-1}$ with $\omega_e x_e$ = 16.3 (37) $cm^{-1}$. The other Raman line, observed at 302.0 $cm^{-1}$, is assigned to the degenerate bending motion $\nu_2(e')$ of the triatomic metal cluster. The frequency ratio of the two fundamentals 432/302 = 1.43 is sufficiently close to $\sqrt{2}$ to indicate that the symmetry of chromium trimer is $D_{3h}$. A summary of our assignment for this spectrum is given in Table 6.1, and values for all spectroscopic constants for this system, namely the ground state vibration for $Cr_3$ ($\omega_e$), the anharmonicity ($\omega_e x_e$), the force constant ($k_e$), and the atomization energy ($D_e^a$) are given in Table 6.2. Note that, as in the dimer, the force constant for the trimer (1.91 mdyne/Å) is rather large, suggesting considerable involvement of d-electrons in the bonding. However, the energy of atomization (0.36 eV) is quite low. Such considerations led Casey and Leopold[4] to suggest that the potential

governing nuclear motions in the dimer deviates considerably from that of a Morse curve. It is likely that such considerations hold for the trimer as well.

**Table 6.1** Summary of observed frequencies for Cr clusters from various laboratories as compared to resonance Raman frequencies obtained via the CCNY metal clusters beam.

| Frequencies ($cm^{-1}$) and assignments for cluster matrix[a] | | Frequencies ($cm^{-1}$) and assignments for mass selected $Cr_3$ (this work). | |
|---|---|---|---|
| 123 | | | |
| 145 | | | |
| 155 | A(0-0) | | |
| 226 | | | |
| | | 302.0 | $\nu_2$ (e') |
| 308 | $\nu_1^{(3)}$ | | |
| 396 | $\nu_1^{(2)}$ | 400.0 | $\nu_1$ ($a_1$) |
| 439 | | | |
| 550 | A(0-1) | | |
| ~620[b] | | | |
| ~770[b] | $2\nu_1^{(2)}$ | 766.1 | $2\nu_1$ |
| ~919[b] | A(0-2) | | |
| ~1100[b] | $3\nu_1^{(2)}$ | 1101.0 | $3\nu_1$ |
| ~1410[b] | $4\nu_1^{(3)}$ | 1439.0 | $4\nu_1$ |

a) See reference 6 and 9. Superscripts (2) and (3) denotes dimer and trimer.
b) Estimated from published spectra in reference 6.

**Table 6.2.** Spectroscopic constants obtained from $Cr_3$ resonance Raman spectra.

| $\omega_e$ ($cm^{-1}$) | $\omega_e x_e$ ($cm^{-1}$) | $D_e$ (eV) | $k_e$ (mdyne/Å) |
|---|---|---|---|
| 432.2 (16) | 16.3 (4) | 0.36 | 1.90 |

We also observe an absorption spectrum for $Cr_3$ in the form of a scattering depletion spectrum, as shown in Fig 6.2. The absorption of $Cr_3$ displays noticeable absorption bands in an exciting region of ~ 400 to 685 nm. The positions of these absorption bands are given in the figure. Plotted parallel with the SDS spectrum for chromium trimer are the resonance Raman excitation profiles of the 400.0 and 302.0 $cm^{-1}$ lines. The excitation profiles show significant resonance Raman enhancement of the 400.0 $cm^{-1}$ line in the absorption region of ~ 461 and 477 nm. We were unable to probe the absorption region between ~ 525 to 575 nm due to the unavailability of dyes in this region. The 302.0 $cm^{-1}$ line, $\nu_2(e')$ vibration, shows relatively strong resonant enhancement at ~ 604 and 647 nm. This indicates the existence of strong vibronic coupling in the excited state of these two optical transitions.[5] This conclusion is also likely for the 477 nm transition.

Upon deposition of $Cr_2$ we found no Raman transitions despite an intensive search across the excitation region. We take this to mean that there is little or no resonance enhancement of the dimer lines. A portion of the absorption (SDS) spectrum is shown for $Cr_2$ in Fig. 6.2. Note there is overlap of dimer and trimer absorption in the region of

**Fig. 6.2** Absorption (SDS) spectrum of $Cr_3$ in argon matrices. The SDS spectrum of $Cr_2$ is also displayed as a miniature.

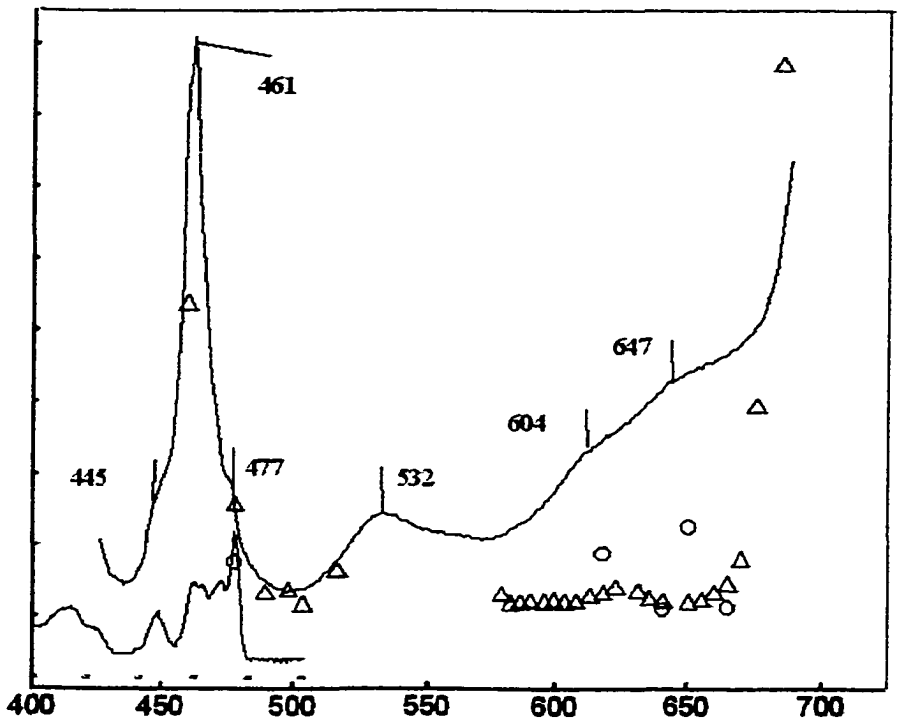

450 to 500 nm, but that the spectra are clearly distinct. There is no measurable intensity for $Cr_2$ at longer wavelengths.

## 6.4 Discussion

Using resonance Raman spectroscopy, DiLella et al.[6] examined a mixture of chromium metal clusters. These molecules were formed by sublimation and subsequent condensation with Ar, Kr, and Xe onto a polished aluminum surface (~ 12 K). Upon excitation at 514.5 nm, DiLella et al. observed 13 spectral lines that we have listed in Table 6.1 along with our results. They found two major progressions that began with fundamentals located in their spectrum at 308 and 396 $cm^{-1}$.[6] One progression (396 $cm^{-1}$) may be characterized by vibrational constants $\omega_e = 427.5$ $cm^{-1}$ and $\omega_e x_e = 15.75$ $cm^{-1}$ and was assigned to the dimer, and the other, based on a line at 308 $cm^{-1}$, gave vibrational constants $\omega_e = 313$ $cm^{-1}$ and $\omega_e x_e = 2$ $cm^{-1}$.[6] Since this latter progression (along with lines at 226 $cm^{-1}$ and 123 $cm^{-1}$) increased in intensity simultaneously upon illuminating a more metal rich portion of the sample, they assigned these lines to the trimer. In addition, a progression with an origin at 155 $cm^{-1}$ was assigned (in a later work) to an excited state (A) of the dimer.[6]

Through pulsed YAG laser vaporization of chromium metal, Bondybey and English[7] observed fluorescence excitation spectrum for $Cr_2$. Based upon their interpretation of the high resolution spectrum, they were certainly viewing emission due to $Cr_2$, i.e. alternate rotational lines were missing from the spectrum, and only the P and R branches were present. From their observed gas phase emission spectrum, Bondybey and English derived $\Delta G_{1/2} = 452.34$ $cm^{-1}$ and a ground state vibrational frequency for the dimer to be $\omega_e \sim 470$ $cm^{-1}$. Our inability to observe resonance Raman intensity in $Cr_2$ is also consistent with their observation that there is practically no change in bond length (0.004 A) in the X to A transition. This would imply extremely small Frank-Condon factors in the resonance Raman spectrum.

The above value for $\omega_e$ was confirmed in the negative ion photoelectron spectroscopy of Casey and Leopold.[8] Their extensive study resulted in the conclusion that the ground state of $Cr_2$ has a potential curve that deviates strongly from a Morse potential. In order to explain the observed vibrational spectrum, they had to assume a "shelf" like addition to the curve and required terms up to order $(v + ½)^6$ to obtain an adequate fit. Their value of $\omega_e = 474.3$ $cm^{-1}$ is in

excellent agreement with that of Bondybey and English and in marked contrast with that of DiLella et al.[6] In a subsequent paper, Moskovits, Limm, and Mejean[9] revisited the spectrum of $Cr_2$ and concluded that the discrepancy between the gas phase results and their matrix isolation results ($\omega_e$ = 425 $cm^{-1}$) are due to an unusually large matrix shift. Usually matrix effects shift observed vibrational frequencies by 1-2 %, so that a shift of almost 10 % must be considered quite large.

Our results presented here clear up this discrepancy. With the advantages provided by mass selection we have shown that, in an argon matrix, $Cr_2$ has no resonance enhancement. The observation by DiLella et al[6] of a progression based on 396 $cm^{-1}$ and attributed to the dimer is nearly identical to the lines observed in our trimer spectrum (Table 6.1). We recommend that our assignment of the 400.0 $cm^{-1}$ progression as the totally symmetric stretch of chromium trimer is indeed the correct assignment for this progression. It is likely that the dimer was not observed by DiLella et al., since we see no resonance enhancement in our mass-selected dimer deposit.

Despite this conclusion, we should note that the analysis of DiLella et al. was strengthened by a careful isotope effect calculation (including the effects of mass on $\omega_e x_e$) of the high resolution spectrum

they attributed to the dimer. A similar analysis for the ($D_{3h}$) trimer failed to fit their observed spectrum. We have been unable to confirm their results since we do not observe these isotopic lines in our spectrum. It is possible that matrix site effects, which were persistent despite their attempts to anneal the sample, complicated their isotopic lines. This explanation requires a rather remarkable coincidence. Despite this discrepancy, we feel that the mass-selection afforded in our experiments remains strong evidence that we are in fact observing the trimer spectrum.

It should be noted that the line we observe at 302.0 $cm^{-1}$, assigned to the e′ vibration, is not the same as that observed by DiLella et al.[6] at 308 $cm^{-1}$. The latter is considerably more intense relative to the 396 $cm^{-1}$in their spectrum. Our observed Raman line at 302.0 $cm^{-1}$ is quite weak, with respect to the 400.0 $cm^{-1}$ line, and has a very different excitation profile (see Fig. 6.2).

In a far IR study of matrix isolated $Cr_3$, Ozin and Mitchell[10] observed over fifteen distinct lines in the range 95 to 325 $cm^{-1}$. They attributed these lines to numerous sites with distinct angular geometries. Since the totally symmetric vibration was not observed in their experiments, they had no independent measure of the stretching

force constant, and assumed $f_r$ = 1.00 mdyne/Å, far lower than we observe here (Table 3). However, our degenerate bending vibration falls within their range of observation. We only see evidence for one site. Because our $Cr_3$/Ar matrix is grown at a much slower rate than that of Ozin and Mitchell[10], most likely our samples had sufficient time to attain the most stable configuration.

In a recent work, Alex, Green, Millam, Villalta and Leopold[11] examined the negative ion photoelectron spectroscopy of mass-selected $Cr_3$. They observed vibrational spacings in the lowest transition of 480(15) $cm^{-1}$ and 130(15) $cm^{-1}$, which differ considerably from the results observed here. Most likely they are observing transitions to a different state than we are, since the geometry derived from these frequencies can not be $D_{3h}$ and the force constants should also be quite different.

Derouault and Dalibart[12] carried out experiments involving acquisition of UV-visible absorption spectra, Raman scattering spectra, and luminescence spectra of highly concentrated chromium fragments vapourized from a tungsten basket and cooled to 12 K in an argon matrix. Using factor analysis methods on the acquired data they resolved the spectra into seven absorption profiles labeled N1 to N7.

Derouault and Dalibart assigned absorption spectra N2, N3, and N4, which gave absorption bands in the 330 nm range, to Cr atoms in different argon sites.[12] Absorption profile N1 was assigned to an excited state of Cr, and absorption spectrum N7 was attributed to $Cr_2$. They made this assignment based on previous absorption profiles obtained by Klotzbücher and Ozin[13] on chromium dimers and trimers in argon matrices. Klotzbucher and Ozin observed low energy optical absorptions for $Cr_2$ at 460/469 nm and for $Cr_3$ at 477 nm.

Comparing our absorption (SDS) profiles for both chromium dimer and trimer to Derouault and Dalibart's absorption spectra N5 (assigned $Cr_3$), N6 (assigned $Cr_2$-Cr), and N7 (assigned $Cr_2$), there are clear similarities. We observe the 469 nm absorption band for $Cr_2$ in our absorption (SDS) spectrum, which they observe in their N6 (assigned $Cr_2$-Cr) absorption spectrum. The 477 nm absorption band that is observed for both chromium dimer and trimer in our absorption (SDS) spectrum is similar to Derouault and Dalibart's N7 (assigned $Cr_2$) absorption spectrum. It is therefore likely that the 477 nm absorption as initially observed and attributed to $Cr_3$ by Klotzbucher and Ozin is correct.[13] This would imply the assignment of spectrum N7 to chromium trimer instead of chromium dimer. This

is also consistent with our reassignment of the Raman spectrum of DiLella et al.[6] This line of reasoning would also imply spectra N5 and N6 to a chromium molecule of higher nuclearity, possibly $Cr_4$, and chromium dimer with a small mixture of the atom respectively.

Clearly, if the above analysis is correct, the lines at 123, 226, and 308 $cm^{-1}$ assigned by DiLella et al.[6], to the trimer of chromium, must be some other species. Since these Raman lines appear in regions of their chromium sample more rich in metal, it is likely that these lines are due to chromium clusters of higher nuclearity. The most likely candidate is the tetramer, $Cr_4$. If the tetramer is a tetrahedron we expect three distinct fundamentals $\nu_1(a_1)$, $\nu_2(t)$, and $\nu_3(e)$, which should have the frequency ratios of $2:\sqrt{2}:1$ respectively.[5] However, $\nu_1/\nu_2 = 308/226 = 1.38$ and $\nu_1/\nu_3 = 308/126 = 2.46$, and thus the tetramer must deviate significantly from a tetrahedral structure. A square planar structure can also be eliminated since all the frequencies should be nearly equal. Another symmetric possibility is a planar rhombus ($D_{2h}$). For such a structure, there should be six distinct fundamentals. Two are of $A_g$ symmetry and should be observed in resonance Raman spectroscopy, while those of $B_{1g}$, $B_{2g}$, and $B_{3g}$ symmetry should be Raman active.

Assuming all bonds have an equal force constant, the frequency ratios for $\nu_1(A_g)$: $\nu_2(A_g)$: $\nu_3(B_{1g})$ should be $3^{1/2}$ / $\sqrt{2}$ / 1, (i.e. 1.73/1.41/1), still considerably different from the observed ratios. Either there is a considerable difference between the rhomboidal diagonal bond force constant and the edge bond force constant, or other possible geometries must be considered. Examining the ratios observed, we might guess that the correct geometry lies somewhere between a rhombus and tetrahedron. We can envision, for example, a planar rhombus in which one atom bends out of plane dihedrally in $C_{2v}$ symmetry until it reaches an apex on top of the remaining three atoms forming a tetrahedron. Normal mode calculations indicate that the vibrational frequencies should vary monotonically between these two limits but, as of now, there is insufficient data observed to obtain a complete analysis. In the two limits, however it is possible to calculate bond stretching force constants assuming the totally symmetric stretch is at 308 $cm^{-1}$. For a tetrahedron we obtain $k_e^{(4)}$ = 1.29 mdyne/Å. For a rhombus (assuming all bonds with equal force constant) $k_e^{(4)}$ = 0.97 mdyne/Å. Using the rules of Ozin and McIntosh[14], as mentioned above, we can predict the expected force constants. For a tetrahedral cluster, $Cr_4$ ($T_d$), we expect $k_e^{(4)} = 1/3\ k_e^{(2)}$

= 1.15 mdyne/Å. For a planar rhombus, $Cr_4$ ($D_{2h}$), we expect $k_e^{(4)}$ = 1/3 $k_e^{(2)}$ (1.15 mdyne/Å) for the diagonal bond and $k_e^{(4)}$ = 2/5 $k_e^{(2)}$ = 1.38 mdyne/Å for the edge bonds.

We see once again that neither the rhomboidal nor the tetrahedral geometry is likely, but that some intermediate ($C_{2v}$) geometry may be correct. Note, however, that the predicted force constants and the observed force constants are sufficiently close in magnitude to lend support for the assignment of these lines to the tetramer. The only other set of metal clusters for which so much information is known about the small cluster force constants is tantalum[5].

**References-Chapter 6**


1. Haouari,H., Wang,H., Craig,R., Lombardi,J.R. and Lindsay,D.M., J.Chem.Phys. ***103***, 9527 (1995). Wang,H., Craig,R., Haouari,H., Lombardi,J.R., and Lindsay,D.M., J.Chem.Phys. ***105***, 5355 (1996). Wang,H., Hu,Z., Haouari,H., Craig, R., Liu,Y., Lombardi,J.R., and. Lindsay, D.M., J.Chem.Phys. 8339, ***106***, (1997). Fang, L., Shen, X., Chen,X., Liu,Y., and Lombardi, J.R., J. Chem. Phys. ***113***, 7178-7181 (2000). Fang, Li, Shen, X., Chen, X., and Lombardi, J.R., Chem.Phys.Lett. ***332***, 299 (2000).

2. Hu, Z.; Shen, B.; Deosaran, S.; Lombardi, J. R.; Lindsay, D. M.; Harbich, W. Proc. SPIE. ***65***, 1559 (1991).

3. Hu, Z.; Shen, B.; Lombardi, J. R.; Lindsay, D. M., J. Chem. Phys. ***96***, 8757 (1992).

4. Casey, S. M.; Leopold, D.G., J. Phys. Chem. ***97***, 816 (1992).

5. Wang,H.,Craig,R., Haouari,H., Dong,J.-G., Hu, Z., Vivoni,A., Lombardi, J.R., and Lindsay, D.M., J.Chem.Phys. ***103***, 3289 (1995), see also Fang,L., Shen, X., Chen,X., and Lombardi, J.R., Chem.Phys.Lett. ***332***, 299 (2000).

6. DiLella, D. P.; Limm, W.; Lipson, R. H.; Moskovits, M.; Taylor, K. V., J. Chem. Phys. ***77***, 5263 (1982).

7. Bondybey, V. E.; English, J. H., Chem. Phys. Lett. ***94***, 443 (1983).

8. Casey, S. M.; Leopold, D.G., J. Phys. Chem. ***97***, 816 (1993).

9. Moskovits, M.; Limm, W.; Mejean, T., J. Phys. Chem. ***89***, 3886 (1985).

10. Ozin, G.A. and Mitchell, S.A., Angew.Chemie Int.Ed.Engl. ***22***, 67 (1983).

11. Alex,S., Green, S., Millam,E.L., Villalta, P.W. and Leopold,

D.G., preprint. See also Proceeding of the 44th ASMS Conference on Mass Spectroscopy and Allied Topics, May 12-16, 1996, Portland, Oregon.

12. Derouault, J.; Dalibart, M. , Z.Phys.D-Atoms, Molecules and Clusters, ***19***, 211 (1991).

13. Klotzbucher, W. E.; Ozin, G. A., J. Am. Chem. Soc. ***100***, 2262 (1978).

14. Ozin, G.A. and McIntosh, D.F., J.Phys.Chem. ***90***, 5756 (1985).

# Bibliography

## References- Chapters 1


1. Huang, W. Y. The total Luminescence Spectrum of Chlorin and Isobacteriochlorin at Low Temperatures. Swiss Federal Institute of Technology: Zürich 1994

2. Rebane, A. "Spectral Hole Burning." www.physics.montana.edu/faculty/rebane October 25, 2000.

3. Völker, S. Annu. Rev. Phys. Chem. 1989, 40: 499-530

4. Hayes, J. M.; Lyle, P. A.; Small, G. J. J. Phys. Chem. 1994, 98 7337

5. Ingle, J. D.; Crouch, S. R. Spectrochemical Analysis. Prentice Hall: Saddle River, NJ 1988

6. Völker, S.; Macfarlane, R. M. IBM J. Res. Develop. 1979, 203 547

7. Devires, H.; Wiersma, D. A. Phys. Rev. Lett. 1976, 36 91. Devires, H.; Wiersma, D. A. Chem. Phys. Lett. 1977, 51 565

8. Bains, S. "New glass allows persistent, high-temperature, spectral hole burning." www.spie.org/web/oer/march/mar98/newglass.html. 2000


References Chapter 3


1. Huang, W. Y.; Wild, U. P.; Johnson, L. W. J. Phys. Chem. **96**, 6189 (1992).

2. Johnson, L. W., Murphy M. D., Pope C., Foresti M., and Lombardi, J. R. J. Chem. Phys. **86**, 4335-4340 (1987).

3. Voelker, S., Macfarlane R. M., Genack, A. Z., and Trommsdorff, H. P. J. Chem. Phys. **67**, 1759-1765 (1977).

4. Voelker, S., and Macfarlane, R. M. Chem. Phys. Lett. **61**, 421-4 25 (1987).

5. Voelker, S., and van der Waals, J. H. Molecular Physics. **32**, 1703-1718 (1976).

6. Jansen, G., Noort, M., van Dijk, N., and van der Waals, J. H. Molecular Physics. **39**, 865-880 (1977).

7. Egorova, G. D.; Solov'ev, K. N.; and Shulga, A. M. Zh. Obshch. Khim. **37**, 357 (1976).

8. Koehler, T. R. J. Chem. Phys. **72**, 3389 (1980).

9. Mathisen, H.; Norman, N.; Pedersen, B. F. Acta Chem. Scand. **21**, 127-135 (1967).

10. Neumann, M. A.; Johnson, M. R.; Radaelli, P. G. to be published.

References Chapter 4

1. Cai, M. F.; Dzugan, T. P.; Bondybey, V. E. Chem. Phys. Lett. **155**, 430-436 (1989).

2. Fu, Z.; Lemire, G. W.; Bishea, G. A.; Morse, M. D. J. Chem. Phys. **93**, 8420-8441(1990).

3. Hu, Z.; Shen, B.; Deosaran, S.; Lombardi, J.; Lindsay, D. M.; Harbich, W. Proc SPIE. **65**, 1559 (1991).

4. Hu, Z.; Shen, B.; Lombardi, J.; Lindsay, D. M. J. Chem. Phys. **96**, 8757 (1992).

5. Ginter, D. S.; Ginter, M. L.; Innes, K. K. Astrophys. J. **139**, 365 (1963).

6. Douglas, M. A.; Hauge, R. H.; Margrave, J. L. J. Phys. Chem. **87**, 2945 (1983).

References-Chapter 5

1. Parker, G. A. Analytical Chemistry of Molybdenum. Springer-Verlag: New York (1983).

2. Bursten B. E.; Cotton F. A.; Hall, M. B. J. Am. Chem. Soc. **102**, 6348-6349 (1980).

3. Atha, P. M.; Hiller I. H.; Guest M. F. Chem. Phys. Lett. **75**, 84-86 (1980).

4. Efremov, Y. M.; Samoilova, A. N.; Kozhukhovsky V. B.; Gurvich, L. V. J. Mol. Spectrosc. **73**, 430-440 (1978).

5. Pellin, M. J.; Foosnaes, T.; Gruen, D. M. J. Chem. Phys. **74**, 5547-5557 (1981).

6. Pellin, M. J.; Foosnaes, T.; Gruen, D. M. ACS Symposium Series. **179**, American Chemical Society: Washington, D. C. (1982).

7. Hopkins, J. B.; Langridge-Smith, P. R. R.; Morse M. D.; Smalley, R. E. J. Chem. Phys. **78**, 1627-1637 (1983).

8. Hu, Z.; Shen, B.; Deosaran, S.; Lombardi, J. R.; Lindsay, D. M.; Harbich, W. Proc. SPIE. **65**, 1559 (1991).

9. Hu, Z.; Shen, B.; Lombardi, J. R.; Lindsay, D. M. J. Chem. Phys. **96**, 8757 (1992).

10. Huaiming, W.; Zhendong, H.; Haouari, H.; Craig, R.; Liu, Y.; Lombardi, J. R.; Lindsay, D. M. J. Chem. Phys. **106**, 8339-8343 (1997).

11. Fang, L.; Shen, X.; Chen, X.; Lombardi, J. R. J. Chem. Phys. **113**, 7178-7181 (2000).

12. Heimbrook, L. A.; Rasanen, M.; Bondybey, V. E. J. Phys. Chem. **91**, 2468-2474 (1987).

13. Simard, B.; Lebeault-Dorget, M. A. ; Marijnissen, A.; ter Meulen, J. J. J. Chem. Phys. **108**, 9668-9674 (1998).

14. Lian, L.; Mitchell, S. A.; Rayner D. M. J. Chem. Phys. **98**, 11637-11647 (1994).

15. Ozin, G. A.; McIntosh, D. F. J. Phys. Chem. **90**, 5756 (1986).

16. Diez, R. P. International Journal of Quantum Chemistry. **76**, 105 (2000).

References Chapter 6

1. Haouari,H., Wang,H., Craig,R., Lombardi,J.R. and Lindsay,D.M., J.Chem.Phys., ***103***, 9527 (1995). Wang,H., Craig,R., Haouari,H., Lombardi,J.R., and Lindsay,D.M., J.Chem.Phys. ***105***, 5355 (1996). Wang,H., Hu,Z., Haouari,H., Craig, R., Liu,Y., Lombardi,J.R., and. Lindsay, D.M., J.Chem.Phys. 8339, ***106***, (1997). Fang, L., Shen, X., Chen,X., Liu,Y., and Lombardi, J.R., J. Chem. Phys. ***113***, 7178-7181 (2000). Fang, Li, Shen, X., Chen, X., and Lombardi, J.R., Chem.Phys.Lett. ***332***, 299 (2000).

2. Hu, Z.; Shen, B.; Deosaran, S.; Lombardi, J. R.; Lindsay, D. M.; Harbich, W. Proc. SPIE. ***65***, 1559 (1991).

3. Hu, Z.; Shen, B.; Lombardi, J. R.; Lindsay, D. M., J. Chem. Phys. ***96***, 8757 (1992).

4. Casey, S. M.; Leopold, D.G., J. Phys. Chem. ***97***, 816 (1992).

5. Wang,H.,Craig,R., Haouari,H., Dong,J.-G., Hu, Z., Vivoni,A., Lombardi, J.R., and Lindsay, D.M., J.Chem.Phys. ***103***, 3289 (1995), see also Fang,L., Shen, X., Chen,X., and Lombardi, J.R., Chem.Phys.Lett. ***332***, 299 (2000).

6. DiLella, D. P.; Limm, W.; Lipson, R. H.; Moskovits, M.; Taylor, K. V., J. Chem. Phys. ***77***, 5263 (1982).

7. Bondybey, V. E.; English, J. H., Chem. Phys. Lett. ***94***, 443 (1983).

8. Casey, S. M.; Leopold, D.G., J. Phys. Chem. ***97***, 816 (1993).

9. Moskovits, M.; Limm, W.; Mejean, T., J. Phys. Chem. ***89***, 3886 (1985).

10. Ozin, G.A. and Mitchell, S.A., Angew.Chemie Int.Ed.Engl. ***22***, 67 (1983).

11. Alex,S., Green, S., Millam,E.L., Villalta, P.W. and Leopold, D.G., preprint. See also Proceeding of the 44th ASMS Conference on Mass Spectroscopy and Allied Topics, May 12-16, 1996, Portland, Oregon.

12. Derouault, J.; Dalibart, M. , Z.Phys.D-Atoms, Molecules and Clusters, ***19***, 211 (1991).

13. Klotzbucher, W. E.; Ozin, G. A., J. Am. Chem. Soc. ***100***, 2262 (1978).

14. Ozin, G.A. and McIntosh, D.F., J.Phys.Chem. ***90***,